1   # Coevolving edge rounding and shape of glacial erratics; the case of Shap granite, UK

2

3   Paul A. Carling[1]

4

5   [1]School of Geography & Environmental Science, University of Southampton, Southampton, SO17
6   1BJ, UK

7

8   *Correspondence to*: Paul A. Carling (p.a.carling@soton.ac.uk)

9

10   **Abstract**

11

12   The size distributions and the shapes of detrital rock clasts can shed light on the environmental history
13   of the clast assemblages and the processes responsible for clast comminution. For example,
14   mechanical fracture due to the stresses imposed on a basal rock surface by a body of flowing glacial
15   ice releases initial 'parent' shapes of large blocks of rock from outcrop, which then are modified by
16   the mechanics of abrasion and fracture during subglacial transport. The latter processes produce
17   subsequent generations of shapes, possibly distinct in form from the parent blocks. Lacking is a
18   complete understanding of both the processes responsible for block shape changes and the trends in
19   shape adjustment with time and distance away from the source outcrop. Field data on edge rounding
20   and shape changes of Shap granite blocks (dispersed by Devensian ice eastwards from outcrop) are
21   used herein to explore the systematic changes in block form with distance from the outcrop.

22

23   The degree of edge rounding for individual blocks increases in a punctuated fashion with the distance
24   from the outcrop as blocks fracture repeatedly to introduce new fresh unrounded edges. In contrast,
25   block shape is conservative, with parent blocks fracturing to produce self-similar 'child' shapes with
26   distance. Measured block shapes evolve in accord with two well-known models for block fracture
27   mechanics — 1) stochastic and 2) silver ratio models — towards one or other of these two attractor
28   states. Progressive reduction in block size, in accord with fracture mechanics, reflects the fact that
29   most blocks were transported at the sole of the ice mass and were subject to the compressive and
30   tensile forces of the ice acting on the stoss surfaces of blocks lying against a bedrock or till surface.
31   The interpretations might apply to a range of homogeneous hard rock lithologies.

32

33   **Short Summary**

34

35   Edge rounding in Shap granite glacial transported boulders is an irregular function of distance from
36   the source outcrop in northern England, UK. Block shape is conservative, evolving according to block
37   fracture mechanics — stochastic and silver ratio models — towards either of two attractor states.
38   Progressive reduction in size occurs to blocks transported at the sole of the ice mass where the blocks
39   are subject to the compressive and tensile forces of the ice acting against a bedrock or till surface.

40

41   **Key words**

42

43   Glacial erratics, erratic rounding, erratic shape, fracture, subglacial

44

45

1 Introduction

The concentration, size, shape, and the degree of rounding of glacial ice-transported blocks of rock may change with distance from the source outcrop. Spatial trends in concentration have been used frequently to indicate preferred ice flow directions (Kujansuu & Saarnisto, 1990; Evans, 2007, Benn & Evans, 2011, p. 675). Concentrated bands of ice-freighted erratics are referred to as 'indicator plumes', 'indicator trains' or 'indicator fans', with concentrations dropping off rapidly outside of the plumes due to ice-flow induced dispersion (Larson & Mooers, 2004). None-the-less, concentration is also sustained by comminution, whereby blocks fracture, or abrade to form smaller blocks and fragments through time and distance from the source outcrop. In contrast to dispersion, there has been less focus on changes in size, shape, and edge-rounding with distance from source (Benn & Evans, 2011). The changes in the shape of blocks are functions of the mechanical properties of the blocks, primarily rock strength and structure, as well as the physical processes promoting comminution. A change in block shape also represents a change in block size. To explore the controls on edge rounding and the shape of erratics, dispersal from a well-known exposure of the Shap granite (Sg) in the UK was examined in the present study. Improved understanding of process controls related to edge rounding and fracture should shed light on the associated basal ice dynamics related to block form changes generally. The two key issues are: 1) the relative importance of fracture mechanics in reducing block size in contrast to edge-rounding and 2) whether edge-rounding and shape coevolve with distance from the source outcrop.

1.1 The Study Area and Context of the Study

The exposure of the Sg pluton occupies a small area (c., 7 km^2) in the eastern English Lake District (Fig. 1) defining a distinct, small, source area for granite blocks. The variation in the concentrations of Sg blocks with distance from the pluton has been used as a key indicator of the directions of ice

74 movement across northern England (reviewed by Carling *et al*., 2013) during the Dimlington Stadial

75 (*c*., 30 ka BP to 14.7 ka BP) within the overall period of the Devensian glaciation (*c*., 33 ka BP to 11.7

76 ka BP). Around the Late Glacial Maximum (LGM: 26.5 ka BP to 19 ka BP, Clark *et al*., 2009), the region

77 was covered by ice, several hundred metres thick (Evans *et al*., 2009), and Sg blocks were entrained

78 from the subglacial bedrock (Ugelvig *et al*., 2016). Long Fell, on the eastern margin of the exposed

79 pluton, is a kilometre-scale rôche moutonnée, severely ice-plucked in the east and south-east at

80 Wasdale Crag (Fig. 1), with smooth, ice-planed surfaces occurring to the north, west and on the

81 summit (point 452m), indicating the erosional effects of moving ice and debris (Hallet, 1981). The

82 west to east change in the style of erosion, from smoothing to plucking, is consistent with ice in the

83 vicinity of the pluton moving predominantly to the east in an early phase (*c*., 29-25 ka BP; Livingstone

84 *et al*., 2012; Merritt *et al*., 2019) of the Dimlington Stadial, and generally northwards across the pluton

85 subsequent to 22 ka BP, *i.e.* towards the end of the LGM (Livingstone *et al*., 2012; Merritt *et al*., 2019);

86 the latter supposition consistent with the W.S.W. to E.N.E. orientation of glacial striations on the

87 pluton (Nicholson, 1868).

88
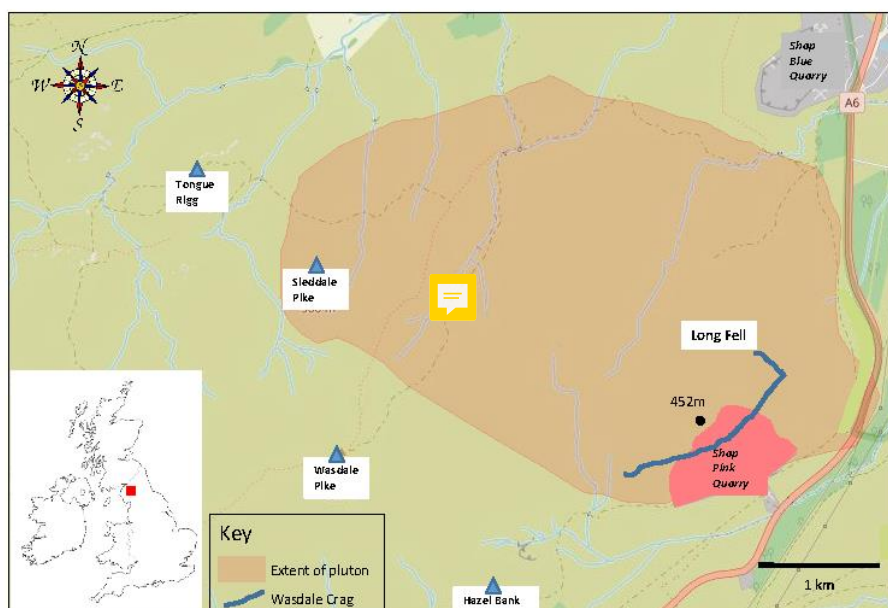
89

90 *Figure 1: Location of the Shap granite pluton. The central portion of the ice-plucked outcrop (Wasdale*
91 *Crag) crag has been destroyed by quarrying. Base map is from CC BY © OS Map Local data.*

In terms of concentration, the dominant dispersal of Sg erratics, during the early phase of the Dimlington Stadial (Stage I; 29-25 ka BP; Merritt *et al*., 2019) was eastward (Carling *et al*., 2013) within sustained ice flow through the topographically controlled corridor of the Stainmore gap across the north Pennines hills (Fig. 2A). The plume extended as far as the east coast of England; a distance more than 100km (Fig. 3). Block size tends to diminish with distance, although examples of far-travelled large blocks occur sparingly (Carling *et al*., 2023). Due to shifting ice divides and competing ice dispersal centres (Merritt *et al*., 2019), subsequently two Sg plumes dispersed in southerly directions until, in the late stadial, erratics briefly were dispersed northwards from the vicinity of the pluton (Carling *et al*., 2013) in accord with the ice movements reported by Livingstone *et al*. (2012). These latter dispersal directions are not considered further herein. The focus solely is on those erratics the final transport vectors (direction and distance) ~~of~~ which are roughly due east, defining a simple linear direction over which changes in the nature of the erratic populations might be measured.

Less well understood than directions of travel and changes in concentration, is the process of edge-rounding and shape changes of Sg blocks that accompany size reduction. The granite is an ideal choice for study as the composition and texture is uniform (Grantham, 1928), mostly giving a massive, unlayered, structure to individual blocks. Layering, such as found within sedimentary rocks, would add complexity to the study of shape evolution, which ~~complexity~~ is avoided in this study. Hopkins (1849) had commented briefly on the rounding of Sg blocks (density ~ 2.61 tonnes m^{-3}) as size reduces towards the east coast, yet such rapid changes in form are seemingly at odds with the high strength of the rock. The strength of Sg in compression exceeds 207 MPa (Holland, 1959;

118
119
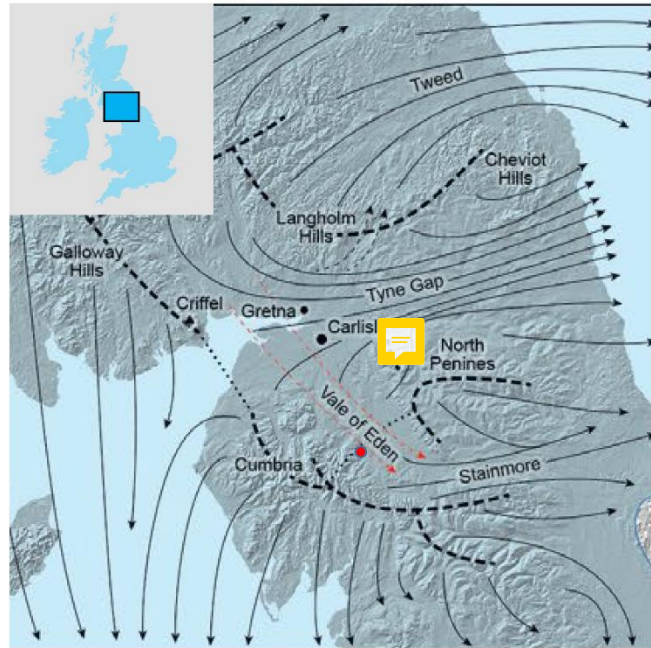
Figure 2: Reconstructed of Stage I (29-25 ka BP) of the last British-Irish Ice Sheet around the Solway Firth (from Merritt et al., 2019. Reproduced with permission) in northern England Stage (inset panel). Eastward ice flow through prominent topographic corridors occurs across the north Pennines. Broken and dotted lines refer to ice divides. Arrows indicate ice-flow vectors (dotted arrows indicate alternative ice-flow scenarios). Topography from NEXTMap digital elevation data. Shap granite erratic plume dispersed to the east from the pluton (red dot) chiefly over Stainmore (see Fig 3).

Day & Goudie, 1977; Goudie, 2006) such that the rock is considered 'very strong' (British Standards,

1981). Despite the rock strength, Hodgson (1870) had remarked on how seemingly rapid rounding of

granite might be aided by rock friability due to a high mica content associated primarily with biotite

(Firman, 1953). Biotite is soft compared with the large phenocrysts of feldspars and quartz (Firman,

1953) that dominate the granite composition. Nevertheless, there has been no investigation of the

changes in shape and rounding of Sg blocks with distance from the source; with very few granite blocks

visually maintaining significant mass over 10's of km. A study of blocks exposed on the modern land

surface, away from major watercourses, should reveal rock-wear processes associated with glacial

transport as there has been negligible losses to Sg surfaces due to post-glacial subaerial weathering

(Wager, 1944; Parsons & Lee, 2005). The few weathered examples of blocks exhibit phenocrysts

standing proud (3-5mm) of the matrix, as the mica is readily subject to chemical weathering if *buried*

5

138   but the feldspars are not much altered (Wager, 1944). —Consequently, an hypothesis was proposed:

139   '*Sg ice-transported blocks would display systematic changes in edge-rounding and shape'*; with an aim

140   *'to demonstrate if edge rounding and shape coevolve with distance to the east from the pluton'.*

141

142
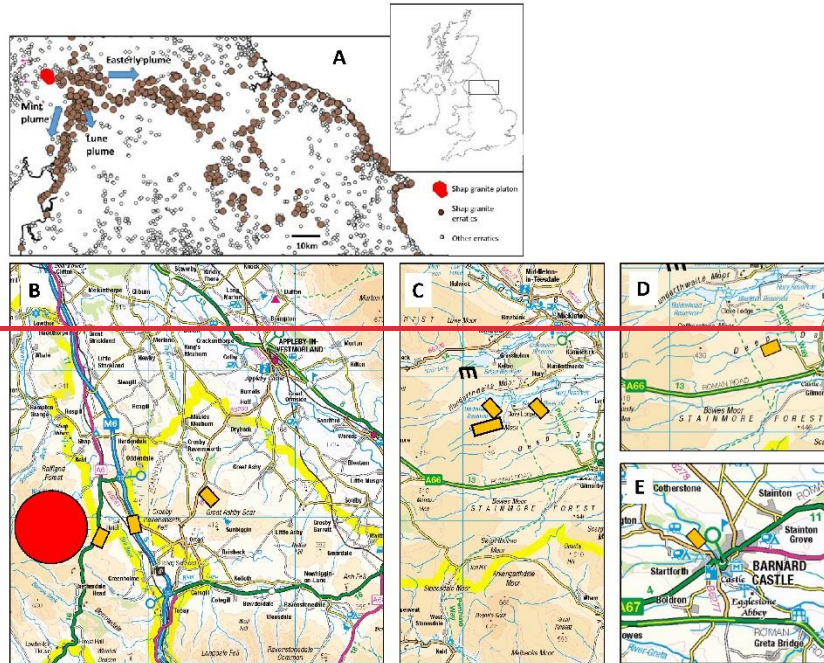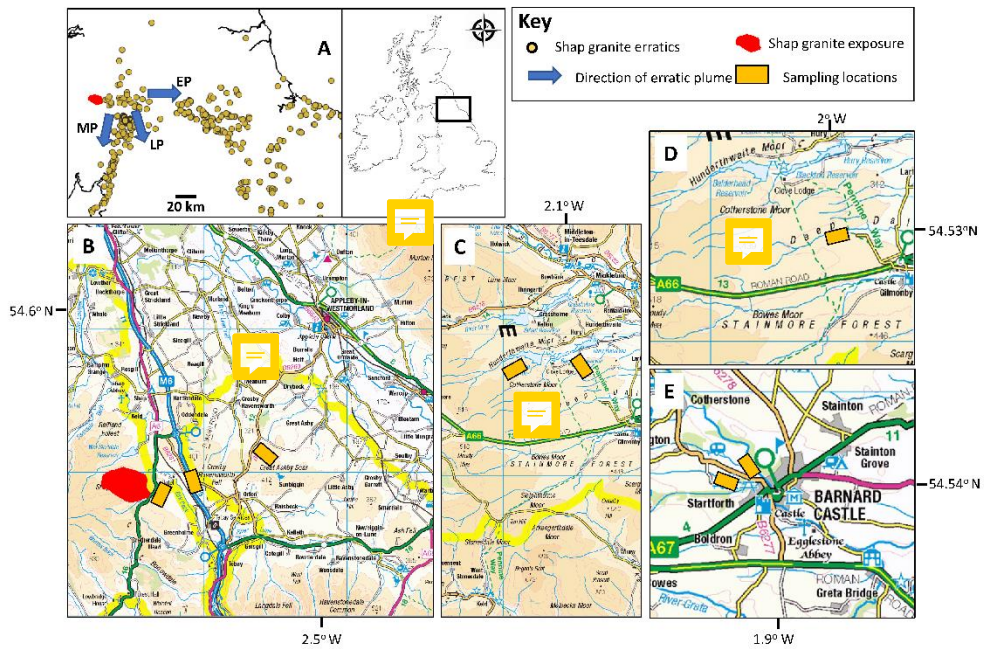
Figure 3: A) Spatial distribution of examples of Shap granite erratics within the study area, northern England (inset), showing the early easterly-directed plume (EP) and, the later southerly Mint and Lune plumes (MP & LP) and subsequent movement of some erratics northwards relative to the source outcrop of Shap granite just east of the pluton. Sampling locations shown Location of sampling sites (yellow rectangles) are indicative of the general sampling areas:; B) Wasdale Bridge, Haybanks, Blasterfield C) upper Teesdale; D) Levy Pool; E) Barnard Castle. See main text for details. Base maps based on CC BY © OS 1:250 000 Scale Colour Raster™.

Shape (and size) changes in a Shap granite block occur due to three predominant processes which scale from effecting small areas of a block to larger areas:

1) abrasion, whereby grain-size fragments (*e.g.,* phenocrysts) are ground-off the block surface (Haldorsen, 1981; Benn & Evans, 2011) primarily by shear stresses associated with blocks moving across a bedrock or till surface in the direction of basal ice motion, or by ice and till moving over stationary blocks lodged against the substratum - this process can result in distinct rounded surfaces on a block (Boulton, 1978; Hallet, 1979);

2) spallation, whereby flakes of rock are freed from the surface of the block (Olsen, 1983) due to externally-derived and internally-derived tensile deviatoric stresses in the rock, both imposed by the motion of the ice overburden, with the shear stresses acting on planes at less than the block scale (Li *et al*., 2018) – this process reduces block mass but results in localized scarred surfaces;

3) fracture (Buscarnera & Einav, 2021) whereby the 'parent' block splits into substantial parts (often two; here referred to as 'child' products). The propagating fissure ultimately may be due to compression loading but, at the block surface, it is the result of a tensile stress (acting on a plane at block scale) flexing the stoss surface of a brittle block lying on a hard basal surface, leading to fissure development often transverse to the direction of basal ice motion (Morland & Boulton, 1975; Hallet, 1996; Benn & Evans, 2011, p264). The tensile strength of a rock is

171   typically an order of magnitude less than the compressive strength (Li *et al.*, 2018). This

172   tripartite classification informed the Method.

173

174 To address the hypothesis, the focus of the study is abrasion and fracture, but observations on

175 spallation were obtained for completeness, with the latter results reported within Supplementary

176 Information. There is justification from studies of bedrock outcrop erosion by basal ice that both the

177 degree of abrasion of bedrock surfaces and the number of fracture events are related to time in

178 transport (Cohen *et al.*, 2006) and thus the distance erratics are moved.

179

2 Method

181

182 Shap granite blocks were sampled along a west to east transect, starting from below Wasdale Crag. It

183 was assumed that all the sampled blocks were from the same population subject to basal traction

184 transport (*vis*. Boulton, 1978) for much of the transport histories; the population being a coarser

185 component of a ~~lodgement~~subglacial traction till ~~till~~(*sensu* Evans *et al.*, 2006) deposited during the

186 waning phase of the easterly phase of ice motion (Fig. 3A) (Hallet, 1979). Blocks ($L > c.$, 1.0 m) were

187 located by field walking. Locations sampled include Wasdale Old Bridge, Haybanks, Blasterfield, sites

188 near Barnard Castle in Teesdale and Levy Pool near Brough (Table S1), respectively 0.8 km, 3.5 km, 8.4

189 km, *c.*, 36 km and *c.*, 41 km from the Wasdale Crag outcrop (Fig. 3). The sites selected were known to

190 have sufficient erratics within defined areas for sampling. However, t~~T~~o obtain similar sample sizes,

191 the areas searched for the final two locations necessarily increased as the surface density of blocks

192 decreased eastwards. Examples of erratics were selected that were sitting on exposed bedrock or till

193 surfaces, so as not to be partially buried. Distance from the source outcrop is assumed to relate to

194 time in transport.

195 At each location, edge, and shape measurements and scar enumeration were made on thirty blocks

196 as briefly described below; the full procedure developed within Supplementary Information. The

197   sample size was found to be sufficient (Daniel, 1999; Conroy, 2018) for the aims of the project and,

198   moreover, interpretation of data trends became possible once the sample size $n > 30$ at each location.

199   These data were supplemented by a regional shape data compendium (Carling *et al.*, 2013). Changes

200   in block size with distance from the pluton are not considered herein using field data, as a statistically

201   significant sample size at each location would have to be prohibitively large to reflect the complete

202   size range of blocks. Rather block size changes are considered within a theoretical framework related

203   to shape changes. Blocks are considered as cuboids consisting of *faces* and *edges*.

204

205   In accord with 1) abrasion: edge rounding was measured after Wentworth (1923; Kirkbride, 1985). In

206   brief, each of the three most tightly rounded edges on the visible portion of each block was defined

207   by a chord (l), delimiting a segment of the block beneath each rounded edge, to give between 80 and

208   90 values for each location. Consideration of the height (h) of the segment in relation to the chord

209   length constrains the radius (r_c) of an inscribed circle beneath the rounded edge, which radius is a

210   measure of the degree of rounding:

211

212   $$r_c = \frac{l^2}{8h} + \frac{h}{2} \qquad\qquad (1)$$

213

214   The radius of curvature reduces as the chord length reduces towards zero and often a right-angle

215   corner occurs when r_c approaches 0. More rounded blocks have larger radii of curvature than less

216   rounded blocks as the sizes of the inscribed circles increase as edges become less sharp. In similar

217   fashion, the edge rounding was measured for joints bounding *in situ* Shap granite blocks constituting

218   the outcrop of Wasdale Crag. These latter data provide a base line of the degree of edge rounding of

219   blocks which have been subject to ice abrasion in place, but without subsequent transport.

220

221   To consider 3) shape changes by fracture: from initial field reconnaissance, blocks close to the source

222   often appear cubic, but polyhedrons occur sparingly - ranging from wedges to prismatoids. Further

223   from the source more ellipsoidal forms are evident. Consequently, to obtain an indication of the shape

224   of a cuboid or an ellipsoid block, the lengths of the three orthogonal axes: long axis (*L*); medium axis

225   (*M*) and the short axis (*S*) were recorded in the field – polyhedrons were not sampled – to give *c*., 30

226   values for each location. Consideration of the mechanics of shape changes also sheds light on the size

227   reduction process with distance. Fracture within individual blocks is sometimes associated with joints

228   and other block-scale planes of weakness. Yet, ice compressive force is the predominant mechanism

229   for significant progressive change in shape for homogeneous granite blocks, inducing tensile fracture

230   and block size reduction. Shape and size changes were examined either via a stochastic fracture model,

231   applicable to fracture at right-angles to either of the *L*, *M* or *S* axes (Domokos *et al.*, 2015) of ellipsoidal

232   blocks or, in accord with the silver ratio model applicable to cuboid blocks fracturing across the *M*-axis

233   alone (Buscarnera & Einav, 2021), as is explained in the Results.

234

235   **3 Results**

236   **3.1 Edge rounding**

237   As is evident from the form of equation 1, rounding is a positive function of the square of the length

238   of the chord of the segment, l, and an inverse function of the segment height, h (Fig. 4). As the

239   inscribed radius values are obtained from both the values of l and h (Equation 1), there is an element

240   of co-variance between the two axes in both panels A and B of Fig. 4. However, plotting the data in

241   this manner allows ready visualization of the trends of the radius data (r_c) relative to the variation in

242   the controlling parameters (l,h). Lower limits to data plotting positions occur in both panels equal to:

243    $r_c = l/2$ and $r_c = h$ respectively.

244   The joint rounding on the pluton is less developed in comparison with the rounding of edges of blocks

245   only 0.8km away at Wasdale Old Bridge (Fig. 4). Although the range in heights of the segments are

246   similar for both locations, the range in chord lengths for the pluton includes smaller values giving

247   overall 'sharper' average edge profiles for the pluton joints in contrast to the Wasdale Old Bridge

248   blocks. It is evident that any 'parent' blocks newly entrained from the outcrop will exhibit both lightly

249   rounded joint edges (glacially abraded when *in situ*) as well as sharp, fresh edges, the latter due to

250   fracture upon release from the outcrop. However, although the initial lightly rounded edges can be

251   further rounded with distance, fracture of entrained blocks introduces new 'sharp' edges as detailed

252   next.

253   Although as distance increases larger radii are more frequent, small radii also occur at distance (Fig.

254   4). It is unlikely that small radii can survive abrasive transport over several 10's of km from the pluton,

255   rather repeated fracture introduces new sharp edges and thus new small radii to different generations

256   of blocks. These new sharp edges begin to round far from the pluton. Although the plots of Fig. 4 are

257   developed considering singular data points from many blocks, if the trends are considered to

258   represent the rounding evolution that would occur for individual blocks, then the black arrows indicate

259   the general direction of edge rounding evolution (*i.e.,* Fig. 4 panel A: if h is constant and l is variable;

260   panel B: if l is constant and h is variable). The linear functions in Fig. 4B allow ready comparison

261   between locations such that, for any value of h, the degree of edge rounding is more pronounced with

262   distance from the pluton; specifically, the linear curves (green, blue, purple, and red) have increasing

263   values of the constant (*i.e*., 1.71, 4.37, 4.69; 5.53 respectively). Similar linear functions for values of l

264   can be applied to Fig. 4A but, for the sake of clarity, these curves are not plotted. The detail of edge
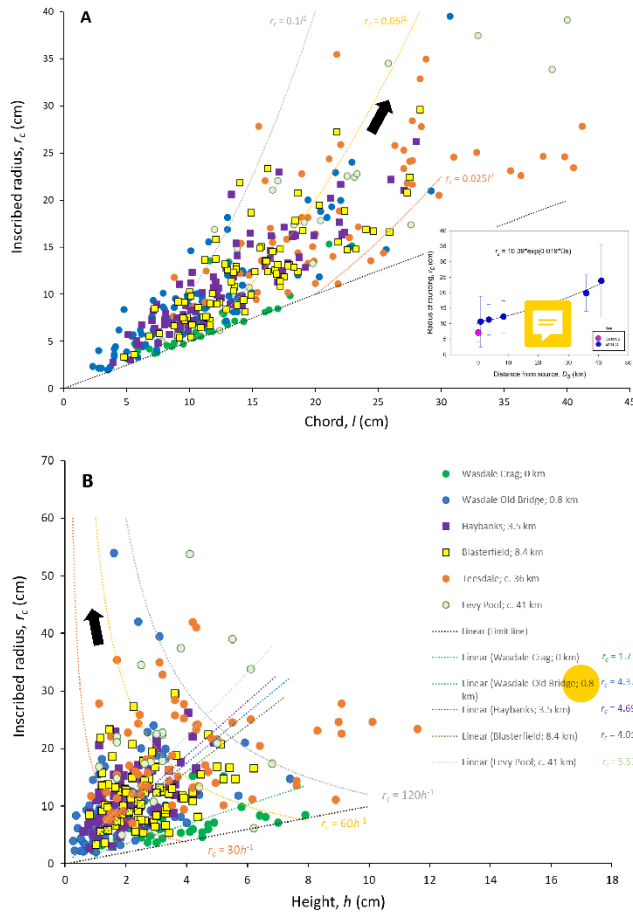
Figure 4: Trends in the values of the inscribed radius as a function of: A) chord length, and; B) segment height. Black arrows indicate the direction of travel of the hypothetical function for an individual block (see main text). Examples of hypothetical curves (brown, yellow and grey) for the trends in individual clast evolution are given for both $r_c \propto l^2$ and $r_c \propto h^{-1}$. Key in panel B also applies to panel A. Inset panel shows mean and s.d. of edge rounding as function of distance from outcrop.

rounding is considered within the Discussion, as edge-rounding of individual blocks is not a smooth

function of distance from the source as might be inferred from the black arrows in Fig. 4 and from the

inset figure of mean edge rounding with distance from the outcrop (Fig. 4 inset panel). The latter

figure depicts an exponential increase in the mean radius of curvature with distance (D_s) from the

source outcrop:

$$r_c = 10.3881e^{(0.0194D_s)}.$$ (2)

3.2 Shape evolution

12

279   In the context of natural hexahedrons, the *stochastic model* of progressive fracture due to the stress

280   of compression (Domokos *et al*., 2015), describes the generation of ellipsoids with the orthogonal axes

281   length proportions: 2.32; 1.52: 1 (Fig. 5A), whereas the *silver ratio* progressive fracture model

282   (Buscarnera & Einav, 2021) describes the generation of cuboids with the edge length proportions: $\sqrt[3]{2^2}$;

283    $\sqrt[3]{2}$; 1, *i.e*.; 1.59: 1.26: 1 (Fig. 6A). In the former model, a fracture plane is orthogonal to any of the

284   three sides of a cuboid (enclosing the ellipsoid) and separates two pieces of equal mass. In the silver

285   ratio model, a fracture plane occurs orthogonal to the current longest axis, separating two pieces of

286   equal mass. In nature, deviation from these two models can occur such that shape self-similarity, in

287   terms of axial ratios, is not maintained necessarily upon successive fracture events if the subsequent

288   fracture is across an axis that differs from the previous fracture event. Fracture across the plane of

289   the short axis was observed in nature (Fig. 5B). However, systematic fracture across the plane of the

290   long axis (Fig. 5C) and across the medium axis (Fig. 5D; Fig. 6B) appeared predominant (*vis* Benn, 1992)

291   for the blocks observed in the field, in accord with both the stochastic and silver models. Given that

292   most blocks rest with the short axis vertical, fracture across the *L* or *M* axes is consistent with known

293   fracture mechanics, whereby the centre of an object is the location, under loading, of the maximum

294   in the tensile stress and the consequent nucleation point for fracture (Hiramatsu & Oka, 1966; Shipway

295   & Hutchings, 1993). From this point, a fracture line develops to the block edges (Man *et al.,* 2018)

296   transverse to the direction of tensile loading. For low values of static or dynamic loading, the rock

297   eventually ruptures into two parts (Man *et al*., 2018). Thus, although a block on occasion might

298   fracture across an axis at variance with the two models above, there is a tendency for blocks to evolve

299   towards one or the other model.   The system state attractors for these two models are shown in Fig.

300   7, wherein natural block shapes are considered. Importantly, compression and tensile fracture leads

301   in both models initially to uniquely defined anisotropic forms, although isotropic forms (*L* = *M* = *S*) can

302   occur in principle with progressive fracture if the fracture rule in each model is relaxed and varied.

303

304
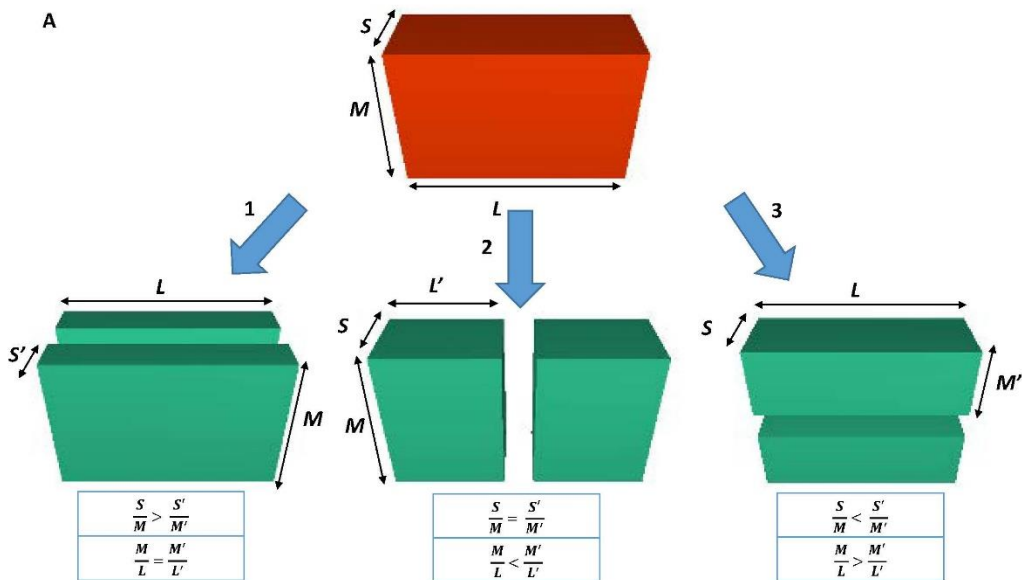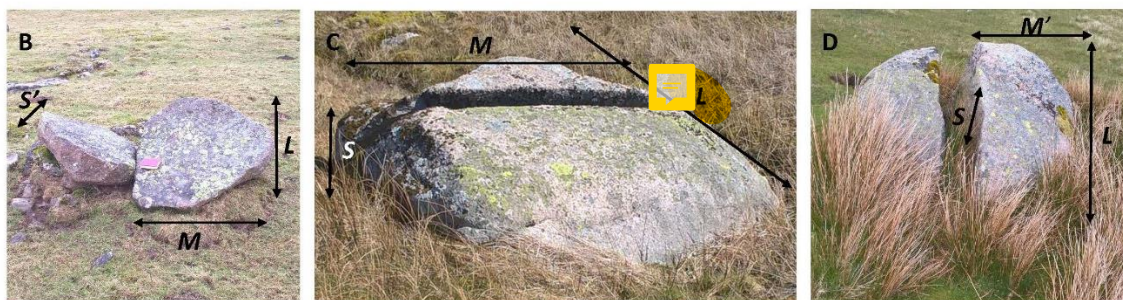
Figure 5: A) Schematic representation of the concept of the stochastic fracture model applied to a three-dimensional cuboid (enclosing an ellipsoid – see Fig. S1) subject to successive fracture given an assumed identical stress loading to the granite block at each fracture event. Fracture planes are orthogonal to a side and separate two pieces of equal mass. Shape self-similarity is not maintained upon successive fracture events. Three different fracture styles are possible within the model, as labelled 1, 2 and 3; B) Example of a well-rounded block split along a fracture plane consistent with model 1; C) Example of a well-rounded block split along a fracture plane consistent with model 2; D) Example of a well-rounded block split along a fracture plane consistent with model 3. The long axes are foreshortened in panels B, C and D.

A

314

B
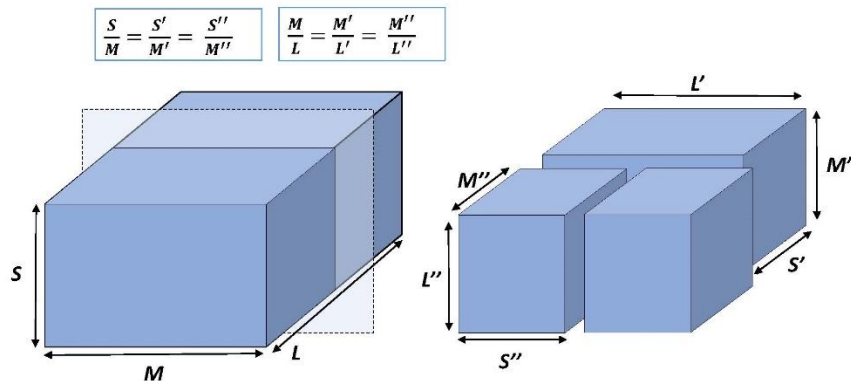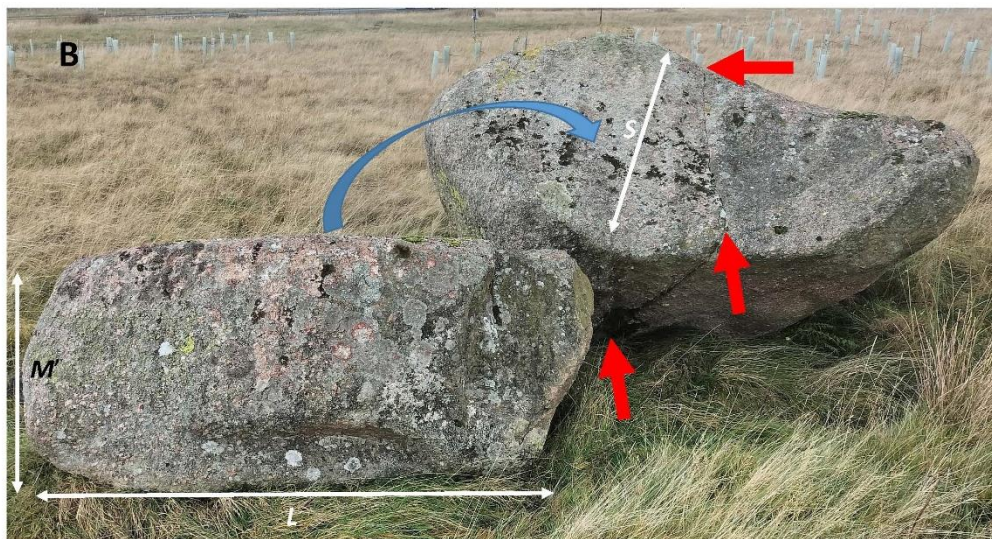

315

316   *Figure 6: A) Schematic representation of the concept of the silver ratio model applied to a three-*
317   *dimensional cuboid (– see Fig. S1) subject to successive fracture given an assumed identical direction*
318   *of stress loading to the granite block at each fracture event. Fracture planes are orthogonal to the*
319   *current long axis. Shape self-similarity is more closely maintained (in contrast to Fig. 5) upon successive*
320   *fracture events; B) Example of silver ratio block. Block to left is approximately the same size as the*
321   *block to the right and the lower surface (not seen) was originally on the top surface of the right-hand*
322   *block with the exposed failure plane bisecting the M-axis alignment of the original parent block. The*
323   *red arrows delineate a fracture plane, aligned with the M-axis of the right-hand block, which divides*
324   *the right-hand block into two near-equal halves.*
325
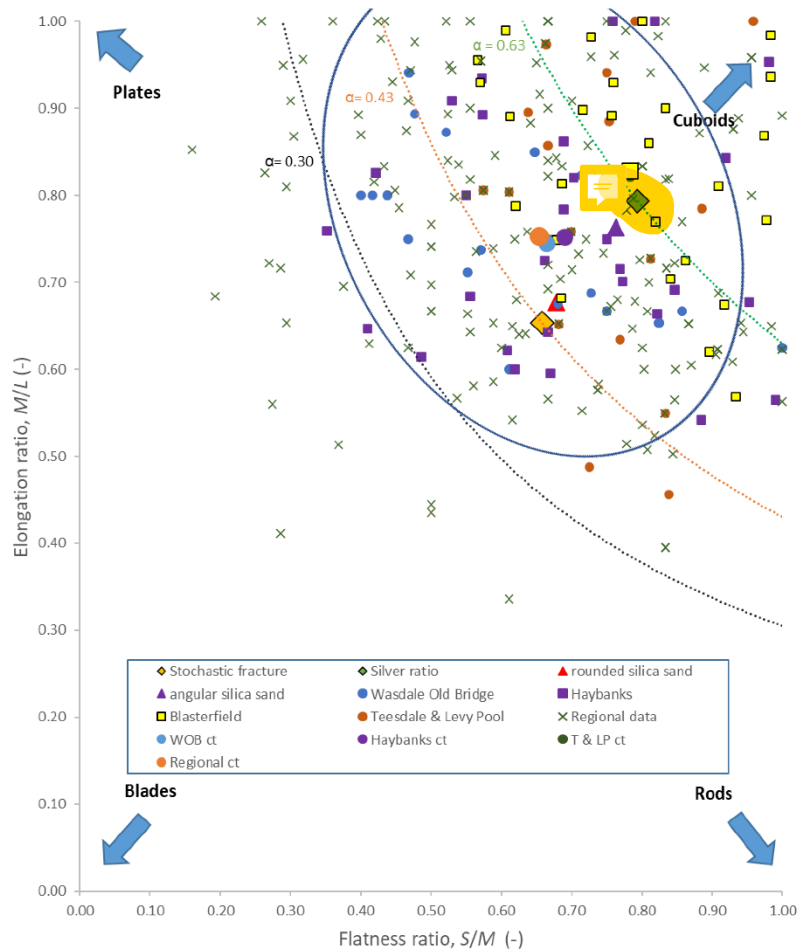
Figure 7: The shape relationship for blocks in terms of the Zingg (1935) ratios. The system state attractors for stochastic fracture (gold diamond) and silver ratio (green diamond) are shown, as are the central tendency shapes for mechanically crushed silica sand grains that were initial sub-rounded or angular (Seo et al., 2021). Curves represent the trend in values of M/L and S/M for constant values of S/L. ct symbols represent the central tendency of each population. Oval is the 95% contour after Oakey et al. 2005.

Within Fig. 7, the Zingg ratios (*S/M and M/L*) for the sampled locations are plotted together with a

data set for the broader region (Regional data). Within Fig. 7, completely equant (isotropic) forms

are absent and plate-like forms survive more readily than rods. Nonetheless, the central tendency of

block shape within the regional data is *S/M* = 0.65 and *M/L* = 0.75; *i.e.*, roughly midway between the

system state attractor for stochastic fracture and the silver ratio attractor. Lines of constant equal

aspect ratios (*S/L*) are shown for the silver ratio model (α = 0.63) and for the stochastic fracture model

(α = 0.43). Seo *et al*. (2021) showed that for homogeneous silica grains, fracture depended on initial

341 particle form (Fig. 7) with angular grains tending towards the silver ratio whilst rounded grains tended

342 towards stochastic fracture. If the fracture process is scale-invariant, then the size differences

343 between silica grains and the Shap blocks can be ignored, and one would expect the Shap granite (a

344 largely homogeneous lithology) to migrate across the diagram from silver to stochastic fracture as

345 cubic blocks become progressively more rounded and ellipsoidal. Blocks deviating from either model

346 (either too long or flat, *e.g.*, approaching α = 0.30), will tend to fracture and migrate back towards α =

347 0.43, as is especially evident in Fig S6B. The central tendencies of the regional data and each of the

348 sampled locations are closely grouped between the central tendencies of the silver and stochastic

349 fracture. The exception is the Blasterfield location which lies closer to the silver ratio, but with

350 increased distance of transport, Teesdale & Levy Pool blocks are in accord with stochastic fracture.

351 Thus, it is evident that block fracture fluctuates between each model, with a trend for constant equal

352 aspect ratios close to α = 0.50 (not plotted in Fig. 7).

353 Although Fig. 7 provides an impression of the spread of block shapes around a central tendency there

354 is no clear impression of the actual shape evolution as possible representative shapes can only be

355 selected arbitrarily from the data clouds. Further, only the cube (or sphere) limit point (*e.g.*, 1, 1 in

356 Fig. 7) is real. Limit points for rods and plates exist only through mathematical definition, because as

357 the rod and plate limit points are approached, rods become infinitely long and plates infinitely thin.

358 Thus, representative shapes need to be selected objectively. To solve this problem the procedure of

359 Oakey *et al*. (2005) was utilized to define representative shapes that define the 95% contour around

360 the central tendency of the regional data, represented by the blue oval in Fig. 7. With reference to the

361 position of the 95% contour in the blade quadrant, curve α = 0.30 is selected to demarcate a lower

362 bound for common block ratios; with a few plate-like or rod-like blocks occurring in the lower portion

363 of the diagram.

364

365 **3.3 Size evolution**

366   The size distribution of the Shap granite blocks with distance from the pluton source has not received

367   detailed attention, although Carling *et al*. (2013) provide some general observations suggesting there

368   is size reduction with distance. In this study, the sample sizes were insufficient to demonstrate the

369   reduction in block size expected with distance from the source outcrop. However, controls on size

370   reduction are evident. Specifically, blocks greater than $L = 4m$ are rare (Carling *et al*., 2013), the size

371   being controlled by the close joint spacing of the granite at source (Firman, 1953). With few

372   exceptions, large blocks ($L > 3.0$ m) do not occur beyond 7 km from the pluton, at which point medium

373   blocks ($2.5 > L > 1.5$ m) become scarce, with small blocks ($1.5 > L > 0.5$ m) and cobble-sized material

374   dominating with further dispersal (Carling *et al*., 2013). These observations indicate that there was a

375   control on the upper size of blocks entrained from the pluton and fracture rapidly reduced block size

376   inducing a crude size-reduction down plume within just a few kilometres. This process was

377   accompanied by local deposition of abrasion and spallation debris as components of a subglacial

378   traction till~~lodgement~~ till. Nevertheless, the fracture mechanics that control block shape inevitably

379   control size evolution (Figs. 5 and 6). For example, fracturing a parent cube with 4m long edges and

380   its progeny across the *L*-axis, only six sequent fracture divisions are required to produce a 1 m cube,

381   as will be demonstrated in the Discussion.

382

383   **4 Discussion: The context of size and shape constraints**

384

385   The initial hypothesis proposed that Sg ice-transported blocks would display changes in edge-rounding

386   and shape with distance to the east from the pluton. As shown in the Results and elaborated below

387   edge-rounding does change with distance but block shape is conservative.

388

389   Space-time substitution is an underlying tenant of this study, in that the size and shape characteristics

390   of multiple individual blocks (an erratic plume), dispersing across the landscape, can reflect the

391   evolution of a single erratic block through time along the same general spatial trajectory. An adequate

392   number of sampled blocks are required for this analogy to hold because perturbations to the

393   population of erratics can occur during dispersal. For example, blocks can have been introduced to

394   the W-E trajectory of the study plume by N-S ice movements reworking blocks previously deposited

395   outside of the eastern-directed plume during periods of time after the main W-E ice flow. Also, for

396   the purposes of determining transport distance, a zero *x*-axis origin has been assumed to be the most

397   easterly outcrop of the pluton at Wasdale Crag. However, some blocks might have been sourced up

398   to a few kilometres to the west of Wasdale Crag. Despite these potential perturbations, which include

399   a small degree of subaerial weathering, the small sample sizes are sufficient to clearly demonstrate

400   systematic change in edge rounding due to ice transport as well as block shape evolution. Finally,

401   edge-rounding and shape are re-set to a degree for the children each time a parent block fractures,

402   so the process of rounding and shape adjustment is not a smooth function of distance from the

403   outcrop, as is explained below.

404

405   **4.1 A conceptual model of block edge rounding controls**

406

407   It should be acknowledged that this study has not considered abrasion of the faces of blocks but has

408   focussed on the edges which tend to abrade and round more rapidly than the associated faces

409   (Boulton, 1974). The edges of blocks still within the outcrop are sharp, albeit some are subject to a

410   slight degree of rounding in place (Fig. 4) from glacial wear, as well as a little post-glacial subaerial

411   weathering. Detached blocks close to the outcrop also tend to exhibit slightly ice-rounded edges, with

412   sharply angled joint planes characterising the other faces due to fracture release of the block from

413   outcrop. The increase in edge rounding with distance confirms the initial hypothesis.

414

415   Block edge rounding initially is constrained by the hardness of the Shap granite and the way it fractures

416   when first entrained at outcrop. The absence of significant edge rounding at the outcrop indicates

417   that blocks were entrained continually until the imposed stresses fell below that required to quarry

418   further blocks. Otherwise, edge rounding of entrained blocks is associated with basal traction

419   transport (Boulton, 1978; Hallet, 1979). Although the compressive strength of granite is high, the

420   tensile strength is an order of magnitude lower; possible as low as 4% of the compressive strength,

421   *i.e.,* 8 MPa (Anikoh *et al.*, 2015; Demirdag *et al.*, 2018; Engineering ToolBox, 2008; Yu *et al.*, 2018).

422   Thus, where compression is translated into flexure, the propensity of the block to elongate across the

423   axis of flexure leads readily to fracture of the brittle granite. This condition means that many blocks

424   close to source initially exhibited near right-angle edges (Fig. 4). Given this geometric constraint, radii

425   of edge curvature inevitable are small initially, approaching the limit: $r_c = l/2$ and $r_c = h$, and

426   increase with distance from the outcrop due to abrasion. However, fracture away from the outcrop

427   introduces new sharp edges (Figs. 4 & 7), such that larger radii characterizing an individual edge-

428   rounded block just before fracture are augmented by smaller radii. This change is reflected in the

429   scatter of radii values found with increased distance from the outcrop (Fig. 4). However, as block size

430   reduces, a condition is approached whereby the population of blocks are increasingly those which

431   resist fracturing (see section 'Block size controls) which should allow edge rounding to become more

432   persistent and thus more pronounced with distance. This condition may be approached in the case

433   of the examples from Teesdale (Fig. 4A) where it is evident that short chords become fewer with

434   distance as larger values of r_c begin to dominate the population. As blocks in transport can reorientate

435   within the ice flow, edge rounding has no effect on block shape, given the shape definition herein.

436   However, if blocks are not free to reorientate, a case not considered herein, the form of blocks can be

437   significantly affected by abrasion in place (Boulton 1974; Hallet, 1979).

438

439   Although a positive exponential function (Equation 2) describes the increase in the mean edge

440   rounding with distance from the source outcrop (Fig. 4A inset panel), the function must eventually

441   transition to a negative function as abraded smaller blocks inevitably are characterized by smaller radii

442   of curvature. This latter condition was not recorded within the current study and sampling at greater

443   distances from the source would be required to determine if this transition occurs. A block (*e.g.*, 1 m

444   cube) subject to edge rounding equally on all 12 edges, as per Equation 2, would have lost about 4%

445   of its mass after 10 km and 9% after 40 km so, in contrast, fracture into two self-similar parts whereby

446   50% of mass is lost, is more significant than edge-rounding in terms of mass loss per block. The greater

447   significance of fracture is consistent with studies of ice erosion by quarrying versus abrasion of basal

448   bedrock surfaces (see references in Cohen *et al*., 2006).

449

450   Rounding of individual bocks is not a steady process, as is evident from the data scatter in Fig. 4 and

451   is further illustrated in the following section. The process whereby the percentage of edges of

452   different generations are rounding with distance, or time, is shown schematically in Fig 8A, wherein

453   there are initially no more than 12 slightly rounded edges to a cube block newly released from outcrop

454   (see Supplementary Information for detail of the model). The model is simple but demonstrates the

455   complexity in edge rounding that must accompany successive fracturing of blocks. Fracturing the

456   block successively across the *L*-axis introduces new generations of fracture edges (sequent fractures

457   – Fig. 8B) at the same time as reducing the number of edges on each new block related to earlier

458   fracture events (see Supplementary Information for further detail). As the number of progeny blocks

459   increases exponentially for each fracture event (Fig. 8C), and each sibling can be further dissected

460   along one, two or three *M*-axes depending on block shape, a diagram including all fracture progeny

461   introduces unreasonable complexity, obscuring the key details. In Fig. 8A&B, for clarity, only one block

462   is followed through one to six sequent fractures, which reduces the number of data points for plotting

463   to a manageable number. The key point to illustrate is that the initial 'parent' block must be fractured

464   five times for one of the ensuing progenies to have lost all the initial 12 edges of the 'parent'. The

465   total number of initial parent edges is relatively persistent because there are 12 edges to begin with

466   (Fig. 8). Contrarily, only four new edges (Fig. 8A) per block are produced on each fracture event. Thus,

467   in contrast to the curve for the initial parent edges, the 1st fracture edges can be lost in as little as four

468   fracture events depending on which sibling block is considered. The 2nd fracture edges are lost by a

total of five fracture events and so on, as more fractures occur adding new fracture edges. Relaxing

the model to allow fracture across either the *M* or *S* axis (see Supplementary Information) only adds

one or two fracture events to the process of edge extinctions. Thus, by introducing new edges at each

fracture event, rounding of the block with distance or time is not a steady progression, with well-

rounded edges being lost as blocks are split at the same time as new immature edges are added to a

population of sub-mature edges. The model may not apply beyond some undetermined number of

fracture events if there is a critical minimum block size that is less susceptible to fracture (as was noted

above) and rounding then can become pronounced. Nonetheless, this model explains the presence

of a 'continuum' from well-rounded edges to less-well-rounded edges on many individual blocks. The

issue as to whether there is a minimum block size is considered in the next section.
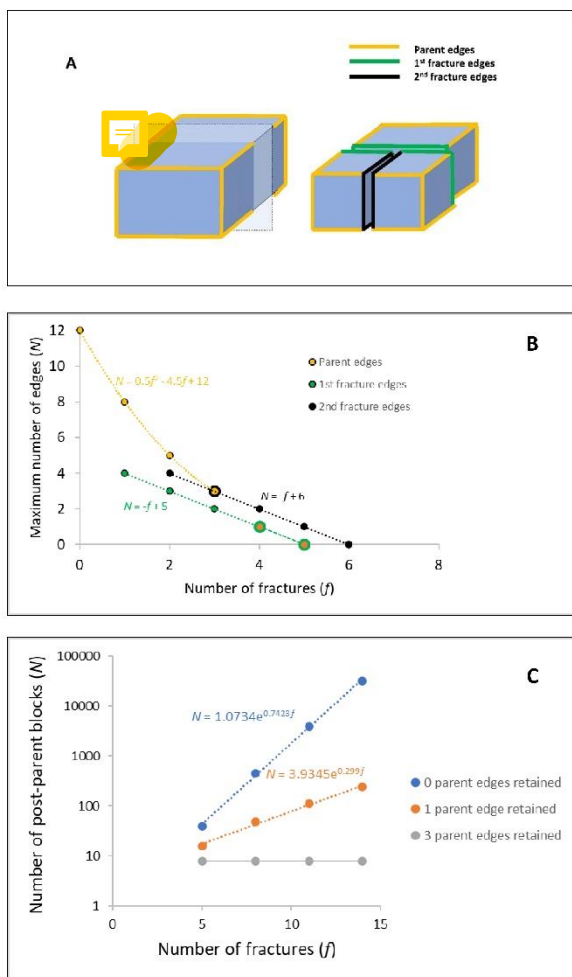
Figure 8: A) A regular block released from outcrop has 12 initial edges (Parent edges) all equally rounded. Fracturing the block at right angles introduces four new edges (1st fracture edges) to each of two sibling blocks, which edges are younger than the initial edges. A further fracture across the L-axis is indicated by 2nd fracture edges; B) The maximum number of edges of each generation on a block as a function of the number of fracture events, with only the parent edges and those edges related to the first two fracture events plotted; C) The total number of blocks created at each fracture event which retain 0, 1 or 3 of the original parent edges.

The significant mean edge rounding, with distance from outcrop (Fig. 4A inset panel), indicates that

the blocks were transported within a mobile concentration of basal debris, in frequent block-to-block

contact and in contact with the bedrock, leading to abrasion before being deposited within a subglacial

traction till~~lodgement till~~ (Hallet, 1979). If the distance travelled towards the east and south is not the

controlling factor, then the high degree of edge-rounding may be due to prolonged temporal transport,

with some material moving east, south, and then north again, extending the transport distances.

However, compatible with studies showing block modification after distances of only 0.4 km (Humlum,

1985; Lliboutry 1994; MacGregor *et al.* 2009), an alternative main explanation is preferred for the

easterly edge-rounding trend. Although Sg is mechanically strong in compression (Goudie, 2006) it is

susceptible to abrasion and tensile fracture for the following reason. The blocks contain large pink

phenocrysts set within a matrix of smaller mineral crystals. The large pink crystals are orthoclase

feldspar (Moh hardness 6 – 6.5). The other common minerals are glassy quartz (Moh hardness 7),

white plagioclase feldspar (Moh hardness 6) and black biotite mica (Moh hardness 2.5 – 3) (Caunt,

1986). ~~Weathered examples of blocks often exhibit phenocrysts standing proud (3-5mm) of the matrix,~~ ~~as the mica is readily subject to weathering (Wager, 1944).~~ Thus, the granular composition of the

granite with harder crystals adjacent to a soft mineral may aid rapid rounding by abrasion and facilitate

tensile facture during glacial transport.

4.2 Block shape controls

Block shape is dependent on the initial controls exhibited at: 1) the outcrop of origin; and 2) the

subsequent transport history.

509

510   1) The primary control is the intersection of sub-vertical joints (Firman, 1953) in the granite with

511   horizontal expansion joint planes caused by unloading (Jahnes, 1943). Horizontal joints largely are

512   due to glacio-isostatic rebound and surface erosion (Westaway, 2009), leading to the release of the

513   residual stresses accumulated at depth (Berger & Pitcher, 1970). The resultant blocks initially tend to

514   be cubic. Where blocks lie within a few metres from the parent outcrop, the block faces tend to be

515   planar, although curved fractured surfaces occur occasionally, as do conchoidal fracture hollows on

516   otherwise planar surfaces. Curved fracture surfaces tend to occur in homogeneous granite due to

517   pressure unloading (Wang *et al*., 2022), which will have occurred as ice erosion reduced the

518   overburden. Such joint-defined blocks within an outcrop are readily entrained by moving ice (Matthes,

519   1930; Morland & Boulton, 1975).

520

521   2) Although inhomogeneous blocks in traction may be envisaged as breaking down into multiple

522   fragments at each compressive event (Boulton, 1978), the largely homogeneous nature of the Sg

523   lithology leads to simple tensile fracturing, at each breakage event, whereby subsequent generations

524   of blocks exhibit shapes largely similar to the parent forms. Thus, there is a tendency for equant blocks

525   to persist, through time and distance, due to the tensile stresses associated with flexure across the

526   stoss surfaces reducing block mass in accord with either the silver model or the stochastic model. This

527   trend is indicated by the fact that stronger plate-like blocks occur less frequently away from the pluton

528   in contrast to the general absence at distance of the weaker rod-like blocks. Thus, cuboids progress

529   to form both cubes and cuboids such that the initial hypothesis is rejected.

530

531   **4.3 Block size controls**

532

533   Block size is dependent on the initial controls exhibited at: 1) the outcrop of origin; and 2) the

534   subsequent transport history.

24

535

536   1) The primary control is the presence of the frequent, well-developed joint planes within the pluton

537   (Firman, 1953; Caunt, 1986) which tend to define and delimit the range of the initial block sizes from

538   *c*., 0.5 m to 4 m. Fault planes are of sufficient rarity to be ignored. Joints are largely orthogonal: *i.e.*,

539   sub-vertical and near horizontal but oblique joints also occur.

540

541   2) Once in ice-transport, other controls on block disintegration may pertain. In the present case,

542   larger blocks close to the outcrop (< 0.8 km) often exhibit one (or more) intact or partially opened

543   failure plane(s) inherited from the outcrop structure. More commonly, with distance from the outcrop

544   (> 0.8 km), the planes of failure within individual blocks represent the directions of tensile and

545   compressive forces exerted by the ice on the blocks (and thus bear no relationship to structure or

546   composition), as appears to be the case where failure planes are aligned with the *L* or *M* axes. Fracture

547   occurred when the effective tensile stress exceeded the yield strength of the blocks. Glacial unloading,

548   and subsequent stress release, also may introduce planes of weakness within transported blocks.

549   Adopting the stochastic fracture mode or the silver ratio model for block shape changes indicates that

550   block volume effectively halves at each fracture event with consequent reduction in block size. This

551   conclusion has implications for the fractal evolution of erratic size distributions which, for brevity,

552   cannot be addressed within this paper.

553

554   Other small-scale planes of weakness can be attributed to spatial variations in the primary mineral

555   composition (Grantham, 1928; Parsons & Lee, 2005) leading to textural and grain-size variations which

556   can be visible rarely as parallel lineaments, and later hydrothermal alteration also induced

557   compositional and hence structural variations (Caunt, 1986). These weaknesses lead to loss of small

558   blocks and flakes from the larger parent blocks (see Supplementary Information) through spallation

559   rather than fracture. Spallation may be related to the state of stress within a deforming till layer

560 (LeBone Hooke & Iverson, 1995) rather than the tensile stress on the stoss side of a block which

561 accounts for block fracture.

562

563 **4.4 General considerations**

564

565 A significant question is whether flowing ice can generate significant stress to fracture the granite

566 blocks. If the thickness of the deforming ice layer at the basal boundary is small relative to the size of

567 the boulder, then the compressive force is likely to dominate. However, if the converse applies then

568 the tensile force likely will dominate. Herein, given that there is no information as to the thickness of

569 the deforming layer, the distinction is not considered because, in most cases, blocks will fracture at a

570 lower stress due to tension in contrast to compression. In a consideration of similar situations,

571 emphasis was placed on the compressive strengths of blocks (Boulton, 1978) relative to the normal

572 stresses due to a static ice load above a block. In the present examples, the tensile strength of the

573 stoss side of a block resisting flexure is more relevant for brittle fracture and for granite can be as low

574 as 8 MPa, which is a tensile stress readily applied by a modest (c., +100m thick) yet dynamic ice cover

575 (Hallet, 1996). The distribution of compressive and tensile forces over the stoss side of a block

576 adjacent to the bedrock at the base of an ice mass will be complex and variable through space and

577 time (Hallet, 1979; Morland & Boulton, 1975; Ficker *et al*., 1980; Cohen *et al*., 2005). Yet, a simple

578 example below outlines the principles within the context of Shap granite erratics. Although a more

579 complex and complete appreciation of the stress environment of a boulder would be preferred, a

580 simple force balance is utilized instead. Simplicity is dictated by the absence of data to inform a more

581 complex model.

582

583 Setting the tensile stress at failure to 8 MPa and treating the rectangular block as subject to a critical

584 average driving force (τ_c) (Benn & Evans, 2011, p.114) due to ice flow, transverse and longitudinal

585 shear stresses arise of equal magnitude. Setting the fracture focus at half the block width in the

26

586 direction of loading, neglecting any water pressure variations (Cohen *et al*, 2006) and deformation

587 within a basal till (LeBone Hooke & Iverson, 1995), and imposing the driving stress transverse to the

588 fracture plane, as little as 180 m thickness (*H*) of flowing glacial ice with an ice surface slope (α) of 1.5°

589 would be sufficient to induce fracture in the block:

590

591 $$\tau_c = \rho_i \, g \, H \, tan \, \alpha, \tag{3}$$

592

593 where ρ_i is the density of glacial ice and *g* is the acceleration due to gravity. The value of *H* = 180 m

594 pertains for a rectangular block with a surface area (*A*) defined by *L* = 2 m and *M* = 2 m (see

595 Supplementary Information for details). The effective instantaneous stress might be greater than as

596 given by Equation 3 (LeBone Hooke & Iverson, 1995) but for a block with *L* = 3 m, *M* = 1 m with the

597 long axis transverse to the ice flow the shear force maximum might be achieved with only 130 m of

598 ice cover (see Supplementary Information). To the east of the pluton the Last British Ice Sheet was

599 several hundred metres thick *c*., 25-22 ka BP (Evans *et al*., 2009), such that blocks would readily

600 fracture during full-glacial warm-based conditions where ice is flowing, as well as after the Late Glacial

601 Maximum when ice was thinning.

602

603 The smallest block sizes (*L* < *c*., 1.0 m) present in the field were not considered, which means that the

604 sampled population was truncated at the finer end. Nevertheless, although in some rock-types, a

605 lower limit to block strength may be related to a minimum structural block size (Dreimanis & Vagners,

606 1971; Lim *et al*., 2004; Domokos *et al*., 2015) this is unlikely to pertain to granite which breaks-down

607 to grus at the scale of the phenocrysts. None-the-less, fracture and surface wear, to an initial block

608 population, tend to result in the observed block population consisting of those blocks which are

609 strongly resistant to further comminution (Moss, 1972; Tavares and King, 1998; Larson & Mooers,

610 2004; Pfeiffer *et al*., 2022) which, in principle, enables some blocks to survive transport adjacent to

611 the sole of the ice for great distances before being deposited during the waning phase of the easterly

612 directed ice stream (Hallet, 1979). Thus, although there may be no lower effective block size, a

613 statistical increase in resistance to fracture of the block population with distance is likely evident as

614 witnessed by the increased rounding seen in the Teesdale population.   The occasional far-travelled

615 large block, as noted in the Introduction, might be explained as being a statistically stronger example,

616 in contrast to the remainder of the population.   Alternatively, large blocks can be cushioned within

617 the till body by smaller particles (Einav, 2007) thus avoiding fracture, or they can be transported

618 englacially, rather than basally, and consequently not subject to protracted abrasion and significant

619 compression whilst in traction. However, englacial blocks are more likely to be angular (Shilts, 1976;

620 Boulton, 1978) and might retain rugose faces.

621

622 Thus, although the reduction in plume parameters values, such as block size and concentration, are

623 commonly viewed as exponential functions of distance from the source (Shilts, 1976), such models

624 (*e.g*., Fig. 4A inset panel) consider the sampled population as a whole and the inferences derived may

625 not apply to the transport history of individual blocks. Certainly, the reduction in edge rounding for

626 individual blocks is irregular with distance.

627

628 **5 Conclusions**

629

630 The hypothesis that granite blocks would display an increase in edge rounding with distance from the

631 source outcrop is confirmed, whilst the hypothesis that shape would evolve with distance is refuted.

632 Although the mean value for edge rounding for the whole block population increases exponentially

633 with distance, edge rounding on individual blocks is an irregular function mediated by block fracture

634 mechanics, as block size reduces (with shapes fluctuating between cuboids, slabs and rods) with

635 distance and new sharp edges are provided to partially edge-rounded blocks. Thus, edge rounding,

636 and shape coevolve as block size is reduced. Fracture transverse to block orientation is in accord with

637 the application of tensile stress which controls the process by which block form is conserved as block

638   size is reduced. Consideration of the orientation of the tensile fractures on blocks in the field might

639   be used to approximate the direction of ice flow at the time of fracture.

640

641   Overall, the results indicate that edge rounding is unlikely to be advanced if blocks continue to fracture.

642   Well-rounded blocks must represent blocks that have resisted splitting. In the case of exceptionally

643   large, rounded blocks, the rock mass likely is unusually homogeneous, lacking potential fracture lines.

644   However, smaller blocks are less likely to contain potential fracture lines and so fracture should

645   become less prevalent as blocks reduce in size, which then promotes edge rounding.

646

647   Future work should consider developing mathematical models that represent the function of edge

648   rounding as predicated by a model (*e.g.*, silver ratio) describing block size reduction. Similar studies

649   considering other lithologies (*e.g.*, stratified sedimentary rocks) likely would find different shape

650   evolution patterns in contrast to the cuboid central tendency displayed by the homogeneous granite,

651   with concomitant implications for edge rounding trends with time and distance.

652

653   **Author contribution**

654

655   PAC designed the study and conducted the field work, analysis, interpretation and drafting.

656

657   **Competing interests**

658

659   The author declares that he has no conflict of interest.

660

661   **Acknowledgements**

662

663   Emma Armstrong (Armstrongs Group) for access to the Shap (Pink) Quarry. Leslie Knight and David

664   Evans (Durham University) provided information on the location of Shap granite erratics in Teesdale

665   and near Levy Pool. Leslie Knight provided the base image for Fig. 3A. Two anonymous referees are

666   thanked for their commentaries which led to improved presentation of the final results.

Data Availability

668   Basic data are available upon reasonable request from the author.

References

672   Anikoh, G.A., Adesida, P.A., Afolabi, O.C.: Investigation of physical and mechanical properties of
673   selected rock types in Kogi State using hardness tests. *Journal of Mining World Express*, 4, 37-51.
674   DOI:10.14355/mwe.2015.04.004, 2015.

676   Benn, D.I. :The genesis and significance of 'Hummocky Moraine': Evidence form the Isle of Skye,
677   Scotland. *Quaternary Science Reviews*, 11, 781-799. https://doi.org/10.1016/0277-3791(92)90083-K,
678   1992.

680   Benn, D.I., Evans, D.J.A.: Glaciers and Glaciation, Hodder, London. 802pp,
681   https://doi.org/10.1111/j.1502-3885.2011.00212.x, 2011.

683   Berger, A.R., Pitcher, W.S.: Structures in granitic rocks: A commentary and a critique on granite
684   tectonics. *Proceedings of the Geological Association of London*, 81, 441–461.
685   https://doi.org/10.1016/S0016-7878(70)80006-2, 1970.

687   Bouchard, M.A., Salonen, V.-P.: Block transport in shield areas, Glacial Indicator Trains, Kujansuu, R.,
688   Saarnisto, M., (editors), Balkema, Rotterdam, 87-107, ISBN 9781003079415, 1990.

690   Boulton, G.S.: Processes and patterns of glacial erosion. Glacial Geomorphology, Coates, D. R.,
691   editor), Binghamton, N.Y., State University of New York, 41-87, Publications in Geomorphology,
692   ISBN: 9789401164931, 1974.

694   Boulton, G.S.: Boulder shapes and grain-size distributions of debris as indicators of transport paths
695   through a glacier and till genesis. *Sedimentology*, 25, 773-799. https://doi.org/10.1111/J.1365-
696   3091.1978.TB00329.X, 1978.

698   British Standard Institution: Code of Practice for Site Investigations, BS 5930
699   HMSO, London, 1981.

701   Buscarnera, G., Einav, I.: The mechanics of brittle granular materials with coevolving grain size and
702   shape. *Proceedings of the Royal Society*, A, 477: 20201005. https://doi.org/10.1098/rspa.2020.1005,
703   2021.

705   Carling, P.A., Su, T., Meshkova, L.: Distribution of Devensian glacial erratics and related evidence
706   elucidate complex ice flow changes across a former ice divide: Northern England. *Proceedings of the
707   Geologists' Association*, 134, 139-165. https://doi.org/10.1016/j.pgeola.2023.01.002, 2013.

708 Caunt, S.L.: Igneous and Metamorphic Processes in the Shap Granite and its Aureole. Unpubl. PhD
709 thesis, University of Leeds, 337pp, https://etheses.whiterose.ac.uk/522/, 1986.
710

711 Clark, P.U., Dyke, A.S., Shakun, J.D., Carlson, A.E., Clark, J., Wohlfarth, B., Mitrovica, J.X., Hostetler,
712 S.W., McCabe, M.: The Last Glacial Maximum. *Science*, 325, 710-714.
713 https://doi.org/10.1126/science.1172873, 2009.
714

715 Cohen, D., Iverson, N.R., Hooyer, T.S., Fischer, U.H., Jackson, M., Moore, P.L.: Debris-bed friction of
716 hard-bedded glaciers. *Journal of Geophysical Research*, 110, doi:10.1029/2004JF000228, 2005.
717

718 Cohen, D., Hooyer, T.S., Iverson, N.R., Thomason, J.F., Jackson, M.: Role of transient water pressure
719 in quarrying: A subglacial experiment using acoustic emissions. J*ournal of Geophysical Research*, 111,
720 F03006, doi:10.1029/2005JF000439, 2006.
721

722 Conroy, R.M., The RCSI Sample size handbook. Technical report, doi: 10.13140/RG.2.2.30497.51043
723 2018.
724

725 Daniel, W.W., Biostatistics: A Foundation for Analysis in the Health Sciences, 7th. New York, John
726 Wiley & Sons, 1999.
727

728 Day, M. J. and Goudie, A. S.: Field assessment of rock hardness using the Schmidt test
729 hammer. *BGRG Technical Bulletin*, 18, 19-29. 1977.
730

731 Demirdag, S., Sengun, N., Ugur, I., Altindag, R.: Estimating the uniaxial compressive strength of rocks
732 with Schmidt rebound hardness by considering the sample size. *Arabian Journal of Geosciences*, 11,
733 502, https://doi.org/10.1007/s12517-018-3847-1, 2018.
734

735 Domokos, G, Kun, F, Sipos, A.A., Szabó, T.: Universality of fragment shapes. *Scientific Reports,* 5,
736 9147. doi:10.1038/srep09147, 2015.

737 Dreimanis, A., Vagners, U.J.: Bimodal distributions of rock and mineral fragments in basal tills. Till: A
738 Symposium, Goldthwait, R.P. (Editor), Ohio State University Press, Columbus, 237-250, ISBN
739 9780814201480 1971.

740 Einav, I.:) Breakage mechanics -Part 1: Theory. *Journal of Mechanics and Physics of Solids*, 55, 1274-
741 1297. https://doi.org/10.1016/j.jmps.2006.11.003, 2007.

742 Engineering ToolBox: *Compression and Tension Strength of some Common Materials*. [online]
743 Available at: https://www.engineeringtoolbox.com/compression-tension-strength-d_1352.html,
744 2008 [Accessed 02 01 2023].

745 Evans, D.J.A.: Glacial erratics and till dispersal indicators. Encyclopaedia of Quaternary Science, S.A.
746 Elias (Editor), Elsevier, Oxford, 975-978, ISBN 978-0-444-52747-9, 2007.

747 Evans, D.J.A., Livingstone, S.J., Vieli, A., O´ Cofaigh, C.: The palaeoglaciology of the central sector of the
748 British and Irish Ice Sheet: reconciling glacial geomorphology and preliminary ice sheet modelling.
749 *Quaternary Science Reviews*, 28, 739-757. doi:10.1016/j.quascirev.2008.05.011, 2009.

750 Evans, D.J.A., Phillips, E.R., Hiemstra, J.F., Auton, C.: Subglacial till: Formation, sedimentary
751 characteristics and classification. *Earth-Science Reviews*, 78, 115-176, 2006.
752 doi:10.1016/j.earscirev.2006.04.001, 2006.

Firman, R. J.: Metamorphism and Metasomatism around the Shap and Eskdale granites, Durham theses, Durham University. http://etheses.dur.ac.uk/9565/, 1953.

Ficker, F., Sonntag, G., Weber, E.: Asätze zur mechanischen deurung der rissentstehung bei parablrissen und sichelbrüchen auf glaziageformten felsoberflächen. *Zeitshcrift für Gletscherkunde und Glazialgeologie,* 16, 25-43, 1980.

Glasser, N.F.; Roman, M.; Holt, T.O.; Žebre, M.; Patton, H.; Hubbard, A.L.: Modification of bedrock surfaces by glacial abrasion and quarrying: Evidence from North Wales. *Geomorphology*, 365, 107283. https://doi.org/10.1016/j.geomorph.2020.107283, 2020.

Goudie, A.S.: The Schmidt Hammer in geomorphological research. *Progress in Physical Geography*, 30, 703-718. https://doi.org/10.1177/0309133306071954, 2006.

Grantham, D.R.: The petrology of the Shap Granite. *Proceedings of the Geological Association*, 39, 299-331. https://doi.org/10.1016/S0016-7878(28)80015-0, 1928.

Haldorsen, S.: Grain-size distribution of subglacial till and its relation to glacial crushing and abrasion. *Boreas*, 10, 91-105. https://doi.org/10.1111/j.1502-3885.1981.tb00472.x, 1981.

Hallet, B.: A theoretical model of glacial abrasion. Journal of Glaciology, 23, 39-50. https://doi.org/10.3189/S0022143000029725, 1979.

Hallet, B.: Glacial abrasion and sliding: Their dependence on the debris concentration in basal ice. *Annals of Glaciology*, 2, 23–28. https://doi.org/10.3189/172756481794352487, 1981.

Hallet, B.: Glacial quarrying: a simple theoretical model. *Annals of Glaciology*, 22, 1-8. https://doi.org/10.3189/1996AoG22-1-1-8, 1996.

Hiramatsu Y, Oka Y.: Determination of the tensile strength of rock by a compression test of an irregular test piece. *International Journal of Rock Mechanics and Mining Sciences & Geomechanic Abstracts,* 3, 89–90. doi:10.1016/0148-9062(66)90002-7, 1966.

Hodgson, E.: The granite drift of Furness. *Geological Magazine*, 7, 328-339. https://doi.org/10.1017/S0016756800209801, 1870.

Holland, E.G.: Shap Granite. *Mine & Quarry Engineering*, 25, 2-15, 1959.

Hopkins, W.: On the transport of erratic blocks. *Transactions of the Cambridge Philosophical Society*, 8, 220-240, 1849.

Humlum, O.: Changes in texture and fabric of particles in glacial traction with distance from source, Myrdalsjokull, Iceland. *Journal of Glaciology,* 31 (108), 150-156. https://doi.org/10.3189/S0022143000006390, 1985.

Jahns, R. H.: Sheet structure in granites, its origin and use as a measure of glacial erosion in New England. *Journal of Geology*, 51, 71– 98, 1943.

Kirkbride, M.P.: Boulder edge-roundness as an indicator of relative age: A Lochnagar case study, *Scottish Geographical Journal*, 121, 219-236, DOI: 10.1080/00369220518737232, 1985.

803 Kujansuu, R., Saarnisto, M.: Glacial Indicator Tracing, Balkema, Rotterdam, 252pp, ISBN
804 9781003079415, 1990.

805

806 Larson, P. C. & Mooers, H. D.: Glacial indicator dispersal processes: a conceptual model.
807 *Boreas*, 33, 238–249. DOI 10.1080/03009480410001262, 2004.

808

809 Le Bone Hooke, R., Iverson, N.R.: Grain-size distribution in deforming subglacial tills: Role of grain
810 fracture *Geology*, 23, 57-60. https://doi.org/10.1130/0091-
811 7613(1995)023%3C0057:GSDIDS%3E2.3.CO;2, 1995.

812

813 Li, X.F., Li, H.B., Zhang, Q.B., Jiang, J.L., Zhao, J.: Dynamic fragmentation of rock material:
814 Characteristic size, fragment distribution and pulverization law. *Engineering Fracture Mechanics*,
815 199, 739-759. https://doi.org/10.1016/j.engfracmech.2018.06.024, 2018.

816

817 Lim, W.L., McDowell, G.R., Collop, A.C.: The application of Weibull statistics to the
818 strength of railway ballast. *Granular Matter*, 6, 229–237. http://dx.doi.org/10.1007/s10035-004-
819 0180-z, 2004.

820

821 Lliboutry, L.L.: Monolithologic erosion of hard beds by temperate glaciers. *Journal of Glaciology*, 40,
822 433-450. https://doi.org/10.3189/S0022143000012314, 1994.

823

824 Livingstone, S.J., Evans, D.J.A., Ó Cofaigh, C., Davies, B.J., Merritt, J.W., Huddart, D., Mitchell, W.A.,
825 Roberts, D.H., Yorke, L.: Glaciodynamics of the central sector of the last British-Irish Ice Sheet in
826 Northern England. *Earth-Science Reviews*, 111, 25-55.
827 https://doi.org/10.1016/j.earscirev.2011.12.006, 2012.

828

829 MacGregor, K., Anderson, R.S., Waddington, E.D.: Numerical modeling of glacial erosion and
830 headwall processes in alpine valleys. *Geomorphology*, 103, 189–204.
831 https://doi.org/10.1016/j.geomorph.2008.04.022, 2009.

832 Man, K., Wang, K., Liu, X.: Dynamic tensile properties of granite varied with depths under a similar
833 loading rate. *Advances in Civil Engineering*, Article ID 6048312,
834 https://doi.org/10.1155/2018/6048312, 2018.

835 Matthes, F. E.: Geological history of the Yosemite Valley. U.S. Geological Survey. Professional Paper
836 160, 160pp, 1930.

837

838 Merritt, J.W., Hall, A.M., Gordon, J.E., Connel, E.R.: Late Pleistocene sediments, landforms and events
839 in Scotland: a review of the terrestrial stratigraphic record. *Earth and Environmental Science*
840 *Transactions of the Royal Society of Edinburgh*, 110, 39-91.
841 https://doi.org/10.1017/S1755691018000890, 2019.

842

843 Morland, L.W., Boulton, G.S.: Stress in an elastic hump: the effects of glacier flow over elastic bedrock.
844 *Proceedings of the Royal Society*, *A,* 344, 157-173. https://doi.org/10.1098/rspa.1975.0096, 1975.

845

846 Moss, A.J.: Technique for assessment of blocks breakage in natural and artificial
847 environments. *Journal of Sedimentary Petrology*, 42, 725–728. https://doi.org/10.1306/74D7261C-
848 2B21-11D7-8648000102C1865D, 1972.

849

850 Nicholson, H.A.: On the granite of Shap, in Westmoreland. *Transactions of the Edinburgh Geological*
851 *Society,* 1, 133-37, https://doi.org/10.1144/transed.1.2.133, 1868.

852

853 Oakey, R.J., Green, M., Carling, P.A., Lee, M.W.E., Sear, D.A., Warburton, J.: Grain-shape analysis– A
854 new method for determining representative blocks shapes for populations of natural grains. *Journal*
855 *of Sedimentary Research*, 75, 1065-1073. https://doi.org/10.2110/jsr.2005.079, 2005.

856

857 Olsen, L.: A method for determining total block roundness in sediments. *Boreas*, 12, 17-21.
858 http://dx.doi.org/10.1111/j.1502-3885.1983.tb00355.x, 1983.

859

860 Pfeiffer, A. M., Morey, S., Karlsson, H. M., Fordham, E. M., & Montgomery, D. R.: Survival of the
861 strong and dense: Field evidence for rapid, transport-dependent bed material abrasion of
862 heterogeneous source lithology. *Journal of Geophysical Research: Earth Surface*, 127,
863 e2021JF006455. https://doi.org/10.1029/2021JF006455, 2022.

864

865 Parsons I., Lee, M.R.: Minerals are not just chemical compounds. *The Canadian Mineralogist*, 43,
866 1959-1992. https://doi.org/10.2113/gscanmin.43.6.1959, 2005.

867

868 Seo, D., Sohn, C., Cil, M.B., Buscarnera, G.: Evolution of blocks morphology and mode of fracture
869 during the oedometric compression of sand. *Géotechnique*, 71, 853-865.
870 https://doi.org/10.1680/jgeot.18.P.300, 2021.

871

872 Shilts, W.W.: Glacial till and mineral exploration. Glacial Till, An Interdisciplinary Study, R.F. Legget
873 (editor), Royal Society of Canada, Special Publication, 12, 205-224,
874 https://doi.org/10.2136/sssaj1977.03615995004100010004x, 1976.

875

876 Shipway P, Hutchings I.: Fracture of brittle spheres under compression and impact
877 loading. I. Elastic stress distributions. *Philosophical Magazine, A* **67**, 1389–1404.
878 https://doi.org/10.1080/01418619308225362, 1993.

879

880 Tavares, L.M., King, R.P.: Single-blocks fracture under impact loading. *International Journal of*
881 *Mineral Processing*, 54, 1–28. https://doi.org/10.1016/S0301-7516(98)00005-2, 1998.

882

883 Ugelvig, S. V., Egholm, D.L., Iverson, N.R.: Glacial landscape evolution by subglacial quarrying:
884 A multiscale computational approach. *Journal of Geophysical Research: Earth Surface*,
885 121, doi:10.1002/2016JF003960, 2016.

886

887 Wager, L.R.: A stage in the decomposition of biotite from the Shap Granite. *Proceedings of the*
888 *Yorkshire Geological Society*, 25, 366-342, 1944.

889

890 Wang, X.-Y., Yin, Y.-C., Xing, M.-L., Zhang, D.-D., Chen, Y., Wang, E.-C.: Microsimulation study on
891 energy release and rock block ejection force of granite under different unloading conditions.
892 *Frontiers in Earth Science*, 10:909371. doi: 10.3389/feart.2022.909371, 2022.

893

894 Wentworth, C.K.: A method of measuring and plotting the shapes of pebbles. *US Geological Society*
895 *Bulletin* 730-C, 91-102. doi: 10.3133/B730C, 1923.

897 Westaway, R.: Quaternary uplift of northern England. *Global and Planetary Change*, 68, 357-382.
898 https://doi.org/10.1016/j.gloplacha.2009.03.005, 2009.

900 Yu, M., Wei, C., Niu, L., Li, S., Yu, Y.: Calculation for tensile strength and fracture toughness of granite
901 with three kinds of grain sizes using three-point-bending test. *PLoS ONE*, 13,
902 e0180880. https://doi.org/10.1371/journal.
903 pone.0180880, 2018.

905 Zingg, T.: Beitrag zur schotteranalyse. PhD thesis, ETH Zurich. https://www.reasher-
906 collection.ethz.ch/handle/20.500.11850/135183, 1935.

Supplementary Information for "Coevolving edge rounding and shape of glacial erratics; the case of Shap granite, UK"

Paul A. Carling

1 Supplementary Method

1.1 Sampling strategy

The locations sampled were known from preliminary investigation to contain large numbers of erratics within reasonably prescribed areas. A minimum of 30 Shap granite erratics at each location were measured which meant >90 edge measurements at each location. Choosing a sample size in advance using statistical theory is not possible as the population of erratics is not known. I chose open heathland sites which are undisturbed, and generally searched 1 to 2 km^2 to find 30 erratics. In that sense the sampling is 100% efficient, *i.e.*, all the erratics ($L > 1$m) present at that location were recorded.

If the sampling is considered as a proportion of the total population (unknown) of Shap granite erratics ($L > 1$ m) spread over the landscape in an easterly direction then, as an axiom, a sample of 100 in 20,000 (*i.e.*, 0.5%) often is considered satisfactory (Daniel, 1999; Conroy, 2018). Carling *et al*., (2023) mapped the location of 10,000 erratics, so if this is the target population then the current study measured around 0.45%, in accord with the axiom, but the true population must be larger.

It was decided that the population sampled would only be acceptable if interpretable patterns arose, as reported in the manuscript. Otherwise, the sampled population would be increased. To enlarge the sample size brings problems, as it would require sampling ever-increasing large geographical areas for each nominal point location (*i.e.,* Wasdale Old Bridge, Haybanks, Blasterfield, sites near Barnard Castle in Teesdale and Levy Pool) which means that any function defined by distance from the granite outcrop would be obscured as the search area increased around each nominal point location. Consideration was given to plotting every point against distance but, in that manner, there are insufficient individual points at all the new nominal point locations. Having a sample within a small geographical area means that each sampled erratic is comparable to its' neighbours within the group and the sample sizes are statistically large enough to compare between groups.

1.2 Spallation

Loss of small fragments occurs on the block surface and can disrupt edge rounding locally, leaving scars, but such losses are difficult to parameterize (Olsen, 1983) and rarely have been addressed. Spallation was estimated by enumerating the number of sharp-edged scars on the exposed surfaces of the edges and faces of each individual block, to give *c.*, 38 values for each location. Although an element of subjectivity is involved, using the same procedure and only one operator should demonstrate any significant differences in block populations.

1.3 Block shape

Shap granite blocks ($L > 1$m) were located in the field and the location recorded using a handheld Garmin gps. Locations sampled include Wasdale Bridge, Green Brow and sites in and around Teesdale, respectively 0.5km, 3.5km and 36-54km eastwards from the Wasdale Crag outcrop (Table S1). As the distance from the source outcrop increased the sampling area necessarily had to increase as the concentration of erratics became more dilute. Examples were selected that were sitting on exposed bedrock so as not to be partially buried. To obtain an indication of the size of the block and its overall shape, the lengths of the three orthogonal axes: long axis (L); medium axis (M) and the short axis (S) were recorded using a taut tape measure. In addition, a data set for the shape of Shap granite blocks

Table S1: General sampling locations

Location	Wasdale Old Bridge	Haybanks	Blasterfield	Goldsborough	Hunder Beck	Barnard Castle	Levy Pool
Northing	54.468994	54.484814	54.497372	54.554919	54.54376	54.546631	54.534203
Westing	2.673856	2.638158	2.565614	2.073394	2.1274	1.934722	2.051856

obtained from across the region, rather than along the easterly transect were available (Carling *et al*., 2023) to augment the transect data. Block shape can be described in terms of the degree of similarity to an oblong for sharp-edged blocks and to ellipsoids for more rounded blocks. In either case, the axes ($L > M > S$) or the semi-axes ($Lr > Mr > Sr$) can be used to define the volume of the oblong or ellipsoid. Oblongs and ellipsoids can be prolate to resemble blades and rods or oblate to resemble plates depending on the values of L, M and S. Cubes or spheres occur when $L = M = S$.
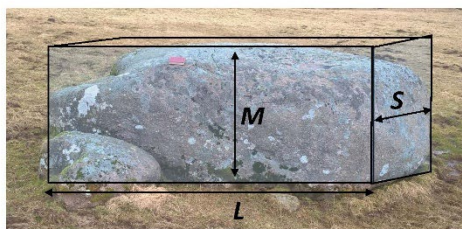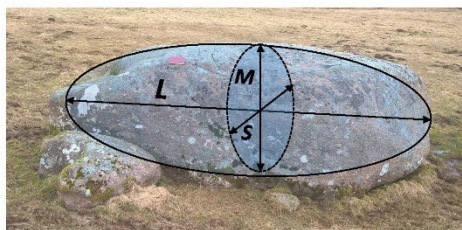
There are various means to describe block shapes and to display such data graphically (*e.g.*, Benn & Ballantyne, 1995; Oakey *et al.*, 2005). In the main text I report the shape indices of Zingg (1935) and use the Zingg projection for its simplicity as data plotted therein show the lack of shape trends clearly. I also considered the Sneed and Folk (1958) shape descriptors, but I did not use their ternary diagram, as the limit points of blades and rods on a Sneed and Folk diagram are so similar as to be indistinguishable. Rather, here in the Supplement I make use of a simple ternary diagram (Hofmann, 1994) relating the readily understandable values of: *L*, *M* and *S*. Once normalized, the values of the axes (*L* > *M* > *S*) can be projected in a ternary diagram to illustrate the shape deviation of each block from the equant shape of a cube or a sphere.

As block shape is defined by the three axes, it would be preferable for graphical plotting if the three parameters could be reduced to two.

Normalization (*N*):

$$N_L = L/(L + M + S)$$

$$N_M = M/(L + M + S)$$

$$N_S = S/(L + M + S)$$

Projections:

$$X = 0.5N_L + N_s$$

$$Y = N_L(COS(30\pi)180)$$

This preference involved recalculating the values of L, M and S to sum to unity. In this manner the shape of each block can be defined as a vector having value and direction (Fig. S2).
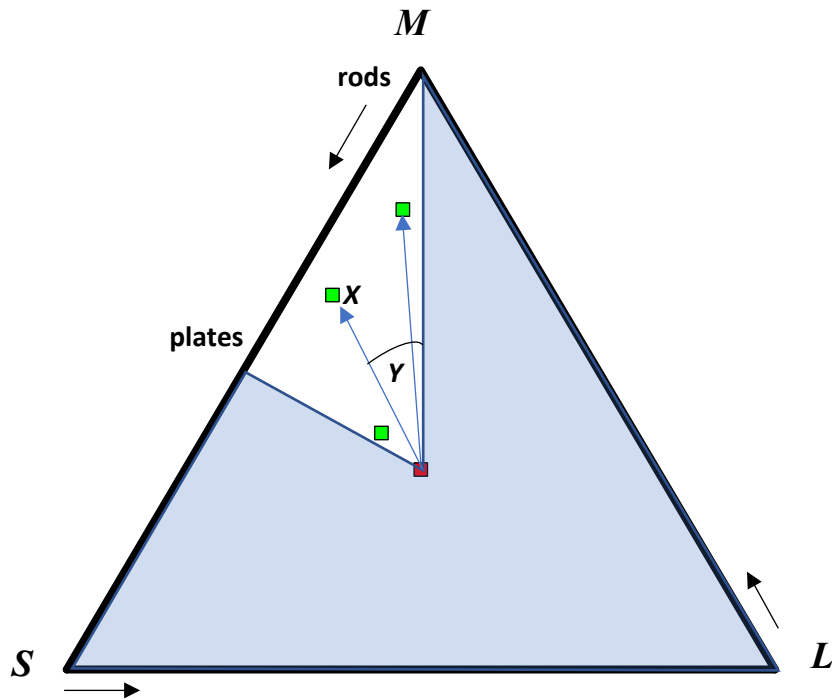
Figure S2: Plot similar to Hofmann (1994), used to define block shape. The normalized values of the semi-axes of three hypothetical blocks (rod, plate, cuboid) are plotted where the value X represents the distance from the centre of the plot where the red symbol represents a sphere. The value Y is equivalent to the angle from the vertical extending from the red symbol to the top vertex. The blue shaded area represents the region in which data cannot exist, give the rule: L > M > S.

Using this method, which is essentially similar to that of Hofmann (1994), the shape of each block readily can be plotted using the two values (X, Y), with blocks deviating from the equant shape of a cube or a sphere with distance away from the centre of the plot. As the distance (X) increases, the block becomes more rod-like but as the angular deviation (Y) increases away from the vertex the blocks become more plate-like. Blocks with small values of X are close to cuboids or spheres.

1.4 Edge rounding

Edge rounding was measured after Wentworth (1923). Where rounded edges were delimited by neighbouring flat facets, the three most prominent rounded edges, delimited by flat facets to either side, were identified by inspection. Two stainless steel straight edges joined by a pivot were used to locate the flat facets either side of the rounded edge (Fig. S3A). A coloured pencil was used to draw a straight line on the block in the plane A, B, C between the intersection points of the two straight planes and the rounded edge. A flexible drafting curve was fitted to the surface of the block between the intersection points (Fig. S3A). In the field, the form of the curve was traced on a sheet of A4 or A3 paper secured to a clipboard. In the office, the rounded segment was defined by a straight line (l) drawn to join the ends of each curve and this length was recorded. The maximum height (h) of the segment was recorded at a right angle to the line, l (Fig. S3). The radius of curvature (r_c) of the inscribed circle within the rounded edge was then determined:

$$r_c = \frac{l^2}{8h} + \frac{h}{2} \qquad\qquad\qquad (S1)$$
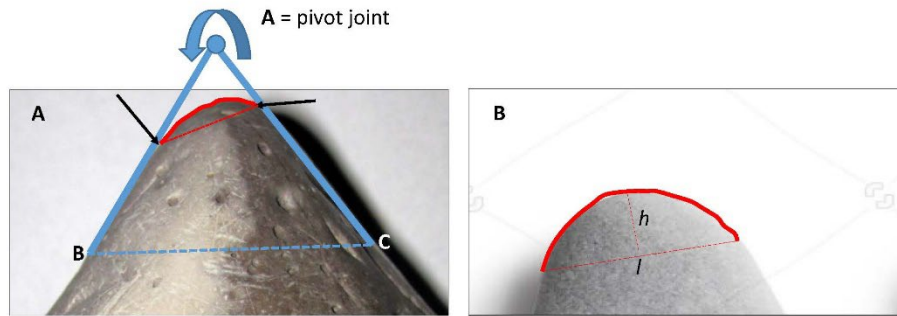

Figure S3: Method used to determine edge rounding in the field. A) Method used for edge rounding arcs, between straight facets. Arrows indicate the intersection points of the curved block surface and constraining straight edges; B) Definition of the method used to define the arc length (l) and the segment height (h). See text for detail.

Silver ratio block edge rounding model

A conceptual model of block rounding

An initial (parent) cube, fracturing across the *L*-axis, fractures to form two oblongs (Fig. S4A). These initial two oblongs each have two equal lengths, so either of these *M*-axes can be selected for further fracture. The subsequent two blocks are oblongs with three unequal lengths each and so there is only one *M*-axis to be selected for fracture. A further third fracture produces two cubes. Thus, four cubes appear after each third fracture in the series. Following this sequence, the initial 12 edges of the initial block reduce to give maximum values of 8, 5, 3, 1 and 0 edges with the initial parent characteristics after each subsequent fracture. The series 12 to 3 can be described by a quadratic equation but this cannot be extended to the 1 and 0 values due to the geometric constraints of the fracture sequence (Fig. S4B). Importantly, blocks with no initial parent edges preserved occur after five fracture events (Fig. S4C).
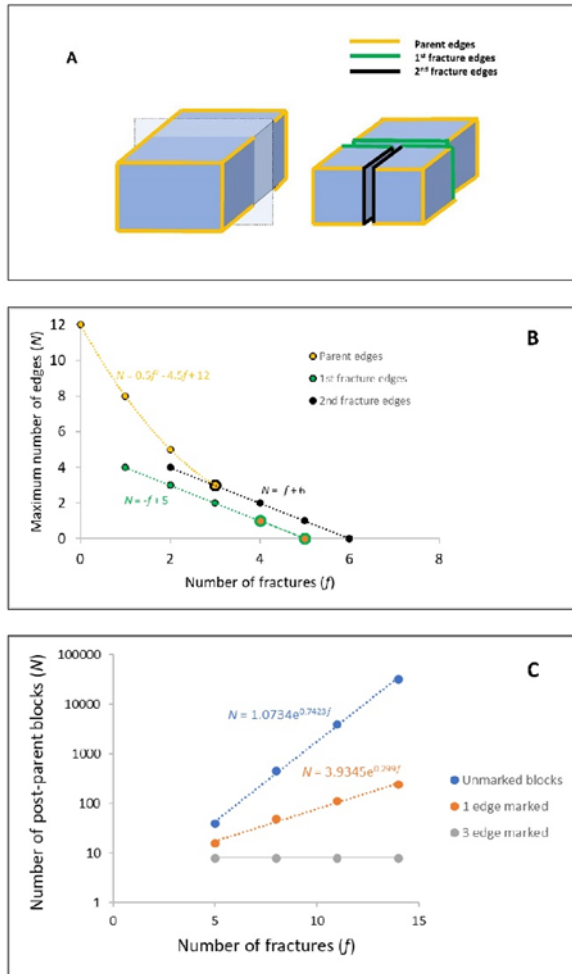
Figure S4: A) A regular block released from outcrop has 12 initial edges (Parent edges) all equally rounded. Fracturing the block at right angles (silver model) introduces four new edges (1st fracture edges) to each of two sibling blocks, which edges are younger than the initial edges. A further fracture is indicated by 2nd fracture edges; B) The maximum number of edges on a block as a function of the number of fracture events, with only the parent edges and those edges related to the first two fracture events plotted; C) The total number of blocks created at each fracture event which retain 0, 1 or 3 of the original parent edges.

The first fracture produces four new edges (to each sibling block), and subsequent fractures reduce these as an arithmetic linear progression: 4, 3, 2, 1 and 0 (Fig. S4B). Each subsequent fracture introduces a new set of four fracture edges which also follow an arithmetic linear progression.

Blocks reduced to display only one initial parent edge can be split to form two blocks, either: A) both having one initial edge, or B) one with an initial edge and one without. Beyond five fractures, the number of blocks displaying no initial edges increases exponentially, more rapidly than the number showing only one edge (Fig. S4C). In principle, four residual blocks will always display three initial edges, but these rapidly become statistically unimportant within the larger population. In the case of cubes, relaxing the rule that the next fracture is at a right angle to the prior fracture (whilst still maintaining blocks of equal mass upon division), three possible orthogonal fracture planes are possible, which is like the stochastic fracture model. When compared to extinction using the rule that fracture is across the *L*-axis, this latter model (not illustrated) can delay the extinction of any edge generation typically by only one or two fracture events.

Treatment of an erratic block as a stationary cuboid subject to flexure failure beneath moving ice

Treating the block as a rectangular body subject to potential bending leading to fracture, the average longitudinal shear force acting on a block with transverse breadth (*L*) and length (*M*) is given simply as:

$$\tau_{av} = \frac{V}{A},$$
(S2)

where *V* is the applied shear force and *A* = *L**M is the area of the block subject to the tangential force of the moving ice. Taking a block with *L* = 2m and *M* = 2m, the on-line calculator for beam forces (Shear Stress Calculator (Beam Analysis); omnicalculator.com) indicates that a shear force of 22 MPa will impose a maximum shear stress τ_{max} at the point of fracture of 8.25 MPa. The peak force (τ_{max}) varies as the ratio of the two axes (*L*, *M*) are varied. For *L* = 3, *M* = 1, the peak force can be *c.*, 1.73 times the average force such that the peak value of 8.25MPa might be achieved when the applied average force is 4.77MPa. Using the shear force values associated with these stress values in Eq. 2, the typical ice thickness ranges from 130m to 180m. Such values are generalizations for illustrative purposes and more complex geometries associated with ellipsoidal erratics would yield somewhat different results.

2 Supplementary Results

2.1 Spallation

Spallation was more evident closer to the source. At Wasdale Old Bridge, only 0.8km from the outcrop, block faces often visually were rugose, even if distinct spallation points were not evident. Spallation on edges was more readily identified than spallation sites on faces. In contrast, with distance from the source, block surfaces tended to exhibit visually smoothed curved surfaces, lacking spallation. Shallow dished scoops occur at distance (from Haybanks eastwards) where spallation points have been smoothed but not removed.
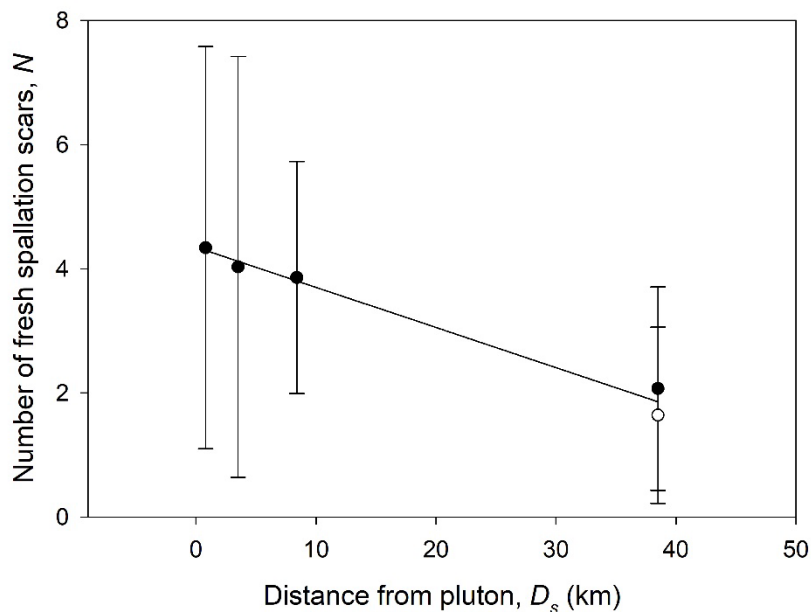
Figure S5: Linear trend in the reduction in the number (N) of fresh spallation scars with distance (D$_s$) from the pluton. At c., 20km scars become more difficult to define, so a maximum estimate (closed symbol) and minimum estimate (open symbol) are included. Error bars are ± 1 standard deviation. Thirty-eight data points in each case, except at 20.5km where the number is 33.

Spallation scars are more prevalent close to the outcrop, where edges are sharp and faces rugose, and are less frequently observed on the smooth rounded block surfaces distal from the outcrop (Fig. S5). Such a negative linear trend in spallation relates to a reduction with distance in the presence of excrescences or microstructural defects, both on edges and on the faces subject to critical ice-loading pressure. Structural failure along a short arc within the excrescent rock mass is more likely than across greater lengths within the block as microstructural defects lead to the propagation of localized fracture (Li *et al*., 2020; Guo *et al*., 2023) until such excrescences are removed. With increased distance from the pluton, there are fewer excrescences and edges are more rounded, so spallation is less frequent and those scars that already exist are abraded smooth. Consequently, spallation is a process that diminishes with distance and is worthy of closer investigation. The present study did not consider the size of spallation scars and a future study might utilize laser scanning to obtain quantitative mass loss data, as the role of spallation in block size reduction has been neglected.

2.2 Block shape

The normalised shapes of blocks are shown in ternary diagrams (Fig. S6). Within Fig. S6A & B, the central triple point is the only location where perfect cubes and spheres can exist. The Wasdale Old Bridge blocks (Fig. S6A), less than 0.8km from the source outcrop, plot close to the triple point, being cubic in form. Yet, many blocks distal from the source (Fig. S6B) still display fairly equant forms. The two green squares, joined by a straight black line represent the arbitrarily selected shape ratios: 3:1:1 and 3:3:1 above which 'limit' more rod-like and plate-like ellipsoid forms occur, albeit scarcely. These results indicates that rod-like and plate-like forms are mechanically unstable, and blocks break down preferentially towards equant forms, which progression indicates that 'parent' blocks, released at the pluton outcrop, tend to spawn 'children' of similar form, which issue is considered next.
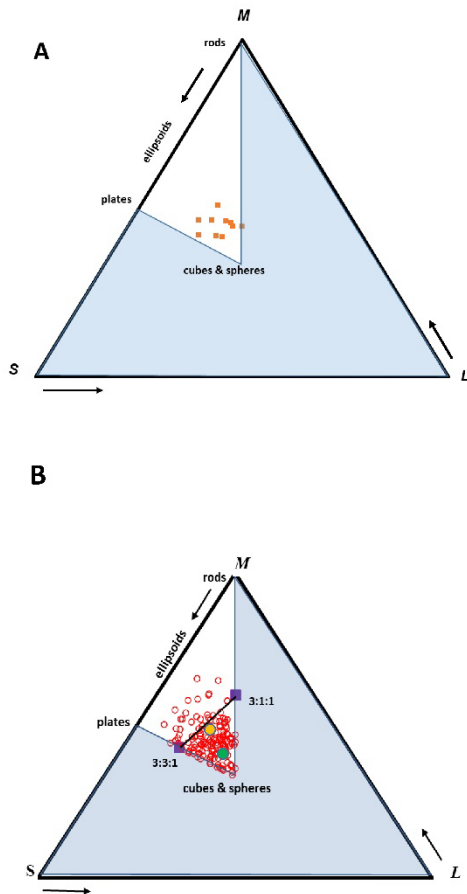
Figure S6: Normalized block axes (values > 0 to < 1) displayed within a Hoffman (1994; 1995) ternary diagram to define block shapes. Given the inequality: L > M > S no data can plot within the shaded portion of the figure. A) Blocks near Wasdale Old Bridge, 0.9km from the source outcrop, cluster close to equant shapes with no examples of prolate (rod) or oblate (plate) forms (n = 28; several coincident points); B) Blocks, 10's of km from source, sampled from across the system show a broader range of shapes, including a few more plate-like and rod-like forms (n = 151). Gold and green symbols are the system state attractors for the fracture model and the silver model respectively (see main text).

References

Benn, D.I., Ballantyne, C.K.: Grain-shape indices and isometric graphs ─ Discussion. *Journal of Sedimentary Research*, A65, 719-721, https://doi.org/10.1306/D42681C6-2B26-11D7-8648000102C1865D, 1995.

Conroy, R.M., The RCSI Sample size handbook. Technical report, doi: 10.13140/RG.2.2.30497.51043 2018.

Daniel, W.W., Biostatistics: A Foundation for Analysis in the Health Sciences, 7th. New York, John Wiley & Sons, 1999.

Guo, P., Zhang, P., Bu, M, Wang, J., Zheng, X., He, M.: Microcracking behavior and damage mechanisms of granite subject to high temperature based on CT-GBM numerical simulation. *Computers and Geotechnics*, 159, 105385, https://doi.org/10.1016/j.compgeo.2023.105385, 2023.

Hofmann, H.J.: Grain-shape indices and isometric graphs. *Journal of Sedimentary Research*, A64, 916-920, https://doi.org/10.1306/D4267F0A-2B26-11D7-8648000102C1865D, 1994.

Hofmann, H.J.: Grain-shape indices and isometric graphs — Reply. *Journal of Sedimentary Research*, A65, 721-723, https://doi.org/10.1306/D42681C6-2B26-11D7-8648000102C1865D, 1995.

Oakey, R.J., Green, M., Carling, P.A., Lee, M.W.E., Sear, D.A., Warburton, J.: Grain-shape analysis– A new method for determining representative blocks shapes for populations of natural grains. *Journal of Sedimentary Research*, 75, 1065-1073, https://doi.org/10.2110/jsr.2005.079, 2005.

Olsen, L.: A method for determining total block roundness in sediments. *Boreas*, 12, 17-21, http://dx.doi.org/10.1111/j.1502-3885.1983.tb00355.x, 1983.

Sneed, E.D., Folk, R.L.: Pebbles in the lower Colorado River, Texas — A study of blocks morphogenesis. *Journal of Geology*, 66, 114-150, 1958.

Wentworth, C.K.: A method of measuring and plotting the shapes of pebbles. *US Geological Society Bulletin* 730-C, 91-102. doi: 10.3133/B730C, 1923.

Zingg, T.: Beitrag zur schotteranalyse. PhD thesis, ETH Zurich, 1935.